This article has been accepted for publication in a future issue of this journal, but has not been fully edited. Content may change prior to final publication. Citation information: DOI 10.1109/TMC.2021.3125201, IEEE Transactions on Mobile Computing

Mobile Measurement of a Dynamic Field via Compressed Sensing

Tianwei Li[1], Qingze Zou[2,⋆]

***Abstract*—In this paper, measuring dynamic signals at points of interest (POIs) using a mobile agent is considered, where the agent is required to repeatedly measure at and transit between the POIs. Dynamic field sensing is needed in areas ranging from nanomechanical mapping of live sample to crop monitoring. Existing work on mobile sensing, however, has been focused on cooperatively tracking one or few known or unknown POIs, whereas the dynamics of the signals is ignored. Challenges arises from capturing and recovering the dynamics at each POI by using data intermittently measured, resulting in temporal-spatial coupling in the mobile sensing. Moreover, trade off between the sensing cost and the performance needs to be addressed. We propose a compressed-sensing based approach to tackle this problem. First, a check-and-removal process based on random permutation and partition of the measurement periods is developed to avoid the temporal-spatial coupling under agent speed constraint. Then a shuffle-and-pair process based on the simulate-annealing is proposed to minimize the transition distance while preserving the performance. It is shown that the distribution of the measurement periods between the POIs converges. The proposed approach is illustrated through a simulation study of measuring the temperature-dependent nanomechanical variations of a polymer sample.**

Keywords: mobile sensing, dynamics mapping, compressed sensing, simulated annealing optimization

I. Introduction

In this paper, the problem of measuring spatial-dependent dynamic processes at multiple points of interest (POIs) using a mobile agent is considered. Such a dynamic mobile sensing is needed in a wide variety of applications, ranging from ocean floor mapping [1] to forestry monitoring [2] and atmospheric circulation monitoring [3]. In these applications, the mobile agent moves between and measures at different POIs. Although the status of interest at each POI can be observed from the sensor data, the *dynamic* evolution at each POI may not be captured by the intermittently acquired data, particularly when the evolutions at these POIs change quickly relative to how often the measurements are taken at each POI intermittently. Measuring dynastic evolution rather than static (or quasi-static) status is important in, for example, agriculture [4] for precision regulation of water, fertilizer, and pesticide use [5]. Alternatively, such an issue of dynamic evolution capture might be mitigated by using enough number of mobile agents of fast mobility. This hardware-enriched approach, however, is practically infeasible due to the cost vs. the field to be covered limitation. Therefore, it is central to be able to capture the dynamics of the sensing processes from the intermittent measured data.

Capturing the dynamics across a 2D- or 3D- field has yet to be addressed in mobile sensing. Although mobile sensing has been investigated for various applications, majority of these works are focused on the use of mobile agents to cooperatively accomplish the mission needed. For example, in coverage control [6], [7] and active information gathering [8], the communication scheme and motion planning of a network of mobile agents is developed for detecting and following a feature or event of interests, where the notion of density function has been explored based on the gradient descent optimization [6], [7] and Lyapunov theory [8], to minimize the sensing cost (e.g., total transition distance of the agents) upon noise/disturbance [6], [7] or agent failures [8]. These methods, however, do not aim to cover the POIs over the entire field, nor to capture the dynamics at all the POIs measured. Sensing over the entire field has been considered in the work of information planning [9] and the mobile crowd sensing [10]. The Although issues due to the sensing field being confined and cluttered [9], or the trade-off between the computational complexity optimization and the sensing cost under limited resource (e.g., onboard power) [10] have been tackled, measuring the dynamics at POIs across the field was not yet considered. As a result, the data acquired may not capture nor be used to recover the dynamics at each POI. Therefore, techniques are needed for mobile sensing of dynamic processes at multiple POIs.

Compressed sensing provides a framework to utilize data sparsity for sensing applications [11], [12]. The CS framework allows us to recover a signal from data acquired at sampling frequency much lower than the Nyquist frequency [11], [13]. The CS-based approach has also been extended to wireless sensor network (WSN) [14], [15], [16], [17], where the data sparsity across the network is explored through the notion of joint sparsity [18], [19], to optimize the sensing cost vs. the quality, or to further consider the agent location- and condition- dependent cost difference [20]. Although the distribution over the entire field can be recovered vis CS-based optimization [11], [12], the dynamic variations at each POI was not considered, and significant temporal error can be induced in the dynamics of the signals measured. Therefore, efforts are needed to extend the compressed sensing to mobile sensing of dynamic signals at multiple POIs.

Challenges arise in the problem of measuring spatial-dependent dynamic processes at multiple POIs using a mobile

[1]Tianwei Li is a PhD student in the Department of Electrical and Computer Engineering, Rutgers University, Piscataway, NJ 08854, USA tianwei.li@rutgers.edu

[2]Qingze Zou is with the Department of Mechanical and Aerospace Engineering, Rutgers University, Piscataway, NJ 08854, USA qzzou@rci.rutgers.edu

agent. First, the spatial-temporal coupling in mobile sensing arises from the need to capture the dynamics at each POI with limited mobile sensing capability—To capture the dynamics at each POI, the mobile agent must measure at each POI at certain time instants. Thus, conflict in mobile sensing arises when the required measurement time instants at different POIs are too close or overlap to each other. Challenge also exists in optimizing the sensing performance such as minimizing the total transition distance while preserving the sensing quality. Moreover, it is critical to ensure that the measurement time is appropriately distributed between the POIs for capturing the dynamics at each POI. These challenges are tackled in the proposed work.

We propose a CS-based approach to achieve dynamics measurement at multiple POIs across a field using a mobile agent. Particularly, the above challenges arising from the limited mobile sensing capability with respect to the "speed" of the dynamics to be measured are addressed. Mainly, our proposed approach possesses the following contributions:

1) The spatial-temporal coupling issue due to the limited mobile sensing capability is resolved. Based on the CS principle (i.e., random sampling) [12], [21], a feasible measurement strategy is obtained through random permutation and partition of the sensing sequence, followed by a check-and-removal process. The obtained strategy specifies the sensing and transition sequence of the agent between the POIs, under the given mobile transition speed constraint.
2) The measurement strategy is optimized by minimizing the sensing cost while preserving the sensing performance. We propose a shuffle-and-pair process based on the simulated-annealing algorithm [22] to trade off the minimization of the total transition distance (i.e., the cost) with respect to the number of measurement periods used for transition (i.e., the more periods used for measurement, the better the performance is).
3) The proposed sensing scheme is analyzed to characterize the distribution of the measurement periods between the POIs. We show that through the proposed method, this distribution converges as the total number of measurement periods increases, and can be tuned and adjusted by choosing the distribution in the initial permutation and partition.
4) Unlike other mobile sensing and CS-based techniques, the proposed approach attains the goal of measuring the dynamics of interest at all given POIs, by ensuring that the sensing sequence at each POI follows, under the mobility (speed) constraint, the random sampling requirement of CS.
5) The proposed approach allows the sensing strategy to be tailored towards the given sensing objectives. Not only can the sensing cost be traded-off with the quality, but also preference can be given towards chosen POIs over others. Such a preference is particularly useful for mapping dynamically heterogenous field.

We illustrate and evaluate the proposed method through a simulation example of measuring the dynamic nanomechanical variations of a heterogenous polymer sample using atomic force microscope (AFM) [23], [24]. The simulation results show that by using the proposed method, the dynamics at each POI can be accurately recovered (with the dynamics measurement error reduced by three to six times otherwise), the total transition distance can be minimized, and the distribution of the measurement periods between POIs can be tuned closely to the desired one.

Notations: In the rest of the paper, $\mathbf{S}$ denotes a finite set of distinct natural numbers, $\mathbf{S} = \{s_i | s_i \in \mathbb{N} : \text{Natural numbers, and } s_i \neq s_j \text{ for } i \neq j\}$, $|\mathbf{S}|$ is the cardinality of $\mathbf{S}$ (i.e., the number of elements in $\mathbf{S}$). For any given set $\mathbf{S}$, $\mathbf{V_S}$ denotes the corresponding vector with elements from $\mathbf{S}$ in ascending order, i.e., $\mathbf{V_S} = \{v_i | v_i \in \mathbf{S}, \text{ and } v_1 < v_2 \cdots < v_{|\mathbf{S}|}\}$, and $\mathbf{e}_N(\mathbf{V_S}) = [0,\ 1, 0, \cdots, 1, \cdots, 0]_{1\times N}$ denotes a $1 \times N$ row vector consisting of only ones and zeros, with ones appearing at entries specified by the vector $\mathbf{V_S}$ of $|\mathbf{V_S}| \leq N$ and $\|\mathbf{V_S}\|_\infty \leq N$, i.e.,

$$\mathbf{e}_N[j] = \begin{cases} 1 & \text{If } j = \mathbf{V_S}[i], \text{ for } i = 1, \cdots, |\mathbf{V_S}| \\ 0 & \text{Otherwise.} \end{cases} \quad (1)$$

Finally, $\langle \mathbf{u}, \mathbf{v} \rangle$ denotes the inner product of vectors $\mathbf{u}$ and $\mathbf{v}$ of the same length.

II. Single Mobile Sensing of Dynamic Field: Problem Formulation

We consider applications of using a mobile agent to measure spatial-dependent dynamic processes at multiple POIs across a 2D/3D field. For example, in nanomechanical mapping of a time-evolving sample using AFM (e.g., the two guard cells during the opening or closing process of a stoma [25], see Fig. 1), the cantilever probe—as the mobile agent—is positioned and used to measure the nanomechanical properties of the sample at a POI (by applying an excitation force to the sample, and measuring the indentation generated along with the force [26], see Fig. 1 (a)), and then repeatedly transited between and measure at the POIs during the entire mapping process (see Fig. 1 (b)). It is needed to quantitatively capture not only the heterogeneous (i.e., location-dependent) properties of the sample, but also their time-elapsing dynamic evolutions at each covered POI [25].

More formally, the task is to measure the dynamic variations of the signals at given N^s number of POIs over a given period of measurement time, $\mathbf{T}^{tot}$, i.e., the dynamics of the signal at each POI over the *entire* period $\mathbf{T}^{tot}$, $d_j(t)$, for $j = 1, 2, \cdots, N^s$ and $t \in [0,\ \mathbf{T}^{tot}]$, is to be measured, where the change of the signal is slow relative to the transition of the mobile agent between the POIs (called the *POI-transition* below), and thereby, can be recovered from the intermittently acquired data. We assume

Assumption 1. *During each between-POI transition, the agent is moving at a constant speed no larger than the maximum transition speed limit v_s.*

By Assumption 1, the agent dynamics is ignored—the agent dynamics can be accounted for in the proposed approach with minor changes. We define:

This article has been accepted for publication in a future issue of this journal, but has not been fully edited. Content may change prior to final publication. Citation information: DOI 10.1109/TMC.2021.3125201, IEEE Transactions on Mobile Computing

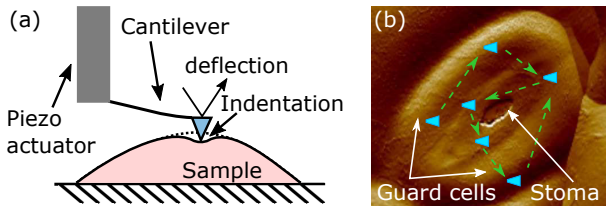

Fig. 1: An example of dynamic field sensing using a mobile agent—Nanomechanical mapping using AFM: (a) the schematic illustration of the indentation-based nanomechanical measurement on AFM; and (b) nanomechanical mapping at multiple POIs of two guard cells during the stoma opening/closing process, where the blue triangles and the green arrowed lines denote the probe measuring at the POIs and the probe transition between the POIs, respectively.

Definition 2. Unit Acquisition Time I^A *The unit acquisition time I^A is the length of the time interval during which the agent R measures at each POI without POI-transition.*

Definition 3. POI-Transition Time $\mathbf{Tr}_{\ell_i,\ell_j}$ *The transition time between any two given i^{th} and j^{th} POIs, ℓ_i and ℓ_j, in the set of POIs $\mathcal{L}_s$ below,*

$$\mathcal{L}_s = \{\ell_1, \ell_2, \cdots, \ell_{N^s} | \ell_i \in \Re^3 : \text{ the coordinate of the } i^{th} \text{ POI}\}, \tag{2}$$

is defined as

$$\mathbf{Tr}_{\ell_i,\ell_j} \triangleq \frac{\|\ell_i - \ell_j\|_2}{v_s}, \tag{3}$$

where v_s is as in Assumption 1.

Definition 4. Minimal and Maximal Transition Time I^T and I^{TX} *The minimal and the maximal transition time I^T and I^{TX} are defined, respectively, as*

$$I^T = \min_{1 \leqslant i,j \leqslant N^s, i \neq j} \mathbf{Tr}_{\ell_i,\ell_j} \tag{4}$$

$$I^{TX} = \max_{1 \leqslant i,j \leqslant N^s, i \neq j} \mathbf{Tr}_{\ell_i,\ell_j}. \tag{5}$$

where $\mathbf{Tr}_{\ell_i,\ell_j}$ is as in Definition 3.

With the above definitions, the total measurement time $\mathbf{T}^{tot}$ can be discretized as

$$N^t = \lfloor \frac{\mathbf{T}^{tot}}{I^M} \rfloor, \quad \text{with } I^M \triangleq I^A + I^T, \tag{6}$$

where $\lfloor a \rfloor$ is the floor function (the largest integer that is not larger than a for $a \in \Re$), i.e., the total measurement period $\mathbf{T}^{tot}$ is now discretized into a sequence $\mathbf{V}_{\mathbf{S}_{tot}}$

$$\mathbf{T}^{tot} \sim \mathbf{V}_{\mathbf{S}_{tot}}, \quad \text{with } \mathbf{S}_{tot} = \{1, 2, \cdots, N^t\}, \tag{7}$$

where $\mathbf{S}_{tot}$ is called the total measurement set.

Definition 5. Discretized Transition Time $D_{tr}(\mathbf{Tr}_{\ell_i,\ell_j})$ *For a given POI-transition time between POIs ℓ_i and ℓ_j, $\mathbf{Tr}_{\ell_i,\ell_j}$, the corresponding discretized transition time $D_{tr}(\mathbf{Tr}_{\ell_i,\ell_j})$ is defined as*

$$D_{tr}(\mathbf{Tr}_{\ell_i,\ell_j}) = \lceil \frac{\mathbf{Tr}_{\ell_i,\ell_j} - I^T}{I^M} \rceil, \tag{8}$$

where $\lceil a \rceil$ is the ceiling function (the smallest integer that is not smaller than a for $a \in \Re$).

Furthermore, we assume that:

Assumption 6. *The number of POIs N^s is much smaller than the total measurement intervals N^t, i.e., $N^s \ll N^t$.*

The above Assumption 6 is to ensure that enough samples are acquired for recovering the dynamics at each POI. Thus, with no loss of generality, we present and discuss this mobile dynamics sensing in discrete-time domain. This discretization scheme implies that any two successive acquisition times are separated by a minimal transition time I^T—Additional time is needed if the transition between two given POIs requires more than the minimal transition time I^T. Thus, it is assumed that

Assumption 7. *The maximum POI-transition time is much smaller than the total measurement time: i.e., the maximum discretized transition time $N^{tr}_{\max}$ satisfies*

$$N^{tr}_{\max} = D_{tr}(I^{TX}) \ll N^t, \tag{9}$$

where $D_{tr}(\cdot)$ is as defined in Eq. (8).

Thus, conceptually the mobile sensing problem considered is to partition the total measurement set $\mathbf{S}_{tot}$ into two subsets each for measurement and transition, respectively, i.e.,

$$\mathbf{S}_{tot} = \mathbf{S}_{\mathcal{M}} \cup \mathbf{S}_{\mathcal{T}}, \tag{10}$$

where $\mathbf{S}_{\mathcal{T}}$ contains the indices of those intervals fully spent on POI-transition (called *transition-only intervals* below), and $\mathbf{S}_{\mathcal{M}}$ contains those used for measurement, respectively. Our goal, thereby, is to maximize and minimize $|\mathbf{S}_{\mathcal{M}}|$ and $|\mathbf{S}_{\mathcal{T}}|$, respectively, while optimizing the measurement under the agent mobility constraint. Formally,

Definition 8. Optimal single mobile sensing of a dynamic field (OSMS-DF) Let Assumptions 1, 6 and 7 hold, then for the POIs given by the set $\mathcal{L}_s$ in Eq. (2) and the measurement interval sequence given by $\mathbf{V}_{\mathbf{S}_{tot}}$ in Eq. (7), the problem of OSMS-DF is to partition and distribute the total measurement set $\mathbf{S}_{tot}$ between all POIs, i.e.,

$$\begin{aligned} &\mathbf{S}_{tot} = \mathbf{S}_{\mathcal{M}} \cup \mathbf{S}_{\mathcal{T}}, \quad \text{with} \quad \mathbf{S}_{\mathcal{M}} \cap \mathbf{S}_{\mathcal{T}} = \emptyset, \text{ and} \\ &\mathbf{S}_{\mathcal{M}} = \bigcup_{i=1}^{N^s} \mathbf{S}_i, \quad \text{with} \quad \mathbf{S}_i \cap \mathbf{S}_j = \emptyset, \\ &\qquad \text{for } \forall 1 \leq i,\ j \leq N^s,\ i \neq j, \end{aligned} \tag{11}$$

where, respectively, $\mathbf{S}_i$ for $i = 1, \cdots, N^s$, is the i^{th} sub-measurement set consisting of the intervals (i.e., their orders) for POI ℓ_i, such that

- $\mathcal{O}_1$ At each POI ℓ_i ($i = 1, 2, \cdots, N^s$), the signal $d_i(t)$ is acquired during the measurement intervals given by the sequence $\mathbf{V}_{\mathbf{S}_i}$, i.e., during each p^{th} interval for $p = \mathbf{V}_{\mathbf{S}_i}[q]$, $g_i[q] = d_i[p]$ is measured for $q = 1, 2, \cdots, N^\ell_i$, with $N^\ell_i = |\mathbf{S}_i|$;
- $\mathcal{O}_2$ When POI-transition is needed, the agent R can be transited from its current POI to the next within the given transition time;

$\mathcal{O}_3$ The dynamic signal at each POI ℓ_i, $d_i[\cdot]$, for $i = 1, 2, \cdots, N^s$, can be recovered from the intermittently measured data, $g_i[\cdot]$, i.e.,

$$d_i[m] \approx \hat{d}_i[m] = F(g_i[1], g_i[2], \cdots, g_i[N_i^\ell]), \quad \text{for } i = 1, 2, \cdots, N^s, \text{ and } m = 1, 2, \cdots, N^t, \tag{12}$$

where $\hat{d}_i[\cdot]$ is the recovered signal, $F(\cdot)$ is the recover (approximation) function used, respectively;

$\mathcal{O}_4$ The total transition distance L_{tot} and the total number of transition-only intervals $|\mathbf{S}_\mathcal{T}|$ is minimized via the following cost function J,

$$\min J = \min\left(c_1 L_{tot} + c_2 |\mathbf{S}_\mathcal{T}|\right), \tag{13}$$

where $c_1, c_2 > 0$ are the corresponding weights, respectively.

Thus, essentially the OSMS-DF problem is to determine an optimal mapping $\mathbb{M}$ from the sequence of measurement intervals, $\mathbf{V}_{\mathbf{S}_{tot}}$ to the sequence of POIs $\mathbf{V}_{\mathcal{L}_s}$, $\mathbb{M}$: $\mathbf{V}_{\mathbf{S}_{tot}} \rightarrow \mathbf{V}_{\mathcal{L}_s}$, to achieve the above objectives $\mathcal{O}_1$ to $\mathcal{O}_4$, i.e., determine a mapping matrix $\mathbb{M}$,

$$\mathbb{M} = \begin{bmatrix} \mathbf{e}_{N^t}(\mathbf{V}_{\mathbf{S}_1}) \\ \mathbf{e}_{N^t}(\mathbf{V}_{\mathbf{S}_2}) \\ \vdots \\ \mathbf{e}_{N^t}(\mathbf{V}_{\mathbf{S}_{N^s}}) \end{bmatrix}_{N^s \times N^t}, \tag{14}$$

where $\mathbf{e}_{N^t}(\mathbf{V}_{\mathbf{S}_j})$s for $j = 1, \cdots, N^s$ are the row vectors defined via Eq. (1). Thus, $\mathbb{M}[j][m] = 1$ indicates that the agent R measures at the j^{th} POI during the m^{th} measurement interval, where $m = V_{\mathbf{S}_j}[p]$ for some index p. We call below the matrix $\mathbb{M}$ a *measurement decision* (MD).

In the above OSMS-DF problem, POI-transition occurs when the next measurement is assigned to a different POI. Thus we define

Definition 9. Transition-Initialization Interval In a given measurement decision $\mathbb{M}$, a given p^{th} measurement interval is a transition-initialization interval if there exists a q^{th} measurement interval, such that $(q-p) > 0$ is the smallest, $p, q \notin \mathbf{S}_\mathcal{T}$, and p, q are not in the same sub-measurement set.

Thus, if the p^{th} interval is a transition-initialization interval, the corresponding POI-transition time is given by

$$\mathbf{Tr}_{p,q} = (q-p)I^M - I^A. \tag{15}$$

Once the MD $\mathbb{M}$ is determined, the measured data at any given j^{th} POI can be readily obtained as

$$g_j = \Phi_j d_j, \tag{16}$$

where for $j = 1, 2, \cdots, N^s$, $\Phi_j \in \Re^{N_j^\ell \times N^t}$ is the sensing matrix for POI ℓ_j that determines the measurement sequence at ℓ_j,

$$\Phi_j[k][m] = \begin{cases} 1 & m = \mathbf{V}_{\mathbf{S}_j}[k] \\ 0 & \text{otherwise,} \end{cases} \quad \text{for } k = 1, 2, \cdots, N_j^\ell, \text{ and } m = 1, 2, \cdots, N^t. \tag{17}$$

We propose to solve the above OSMS-DF problem by using the compressed sensing approach [11], [12]. Particularly, provided that the dynamic signal $d_j[\cdot]$ is sparse in some transformed domain, i.e., the vector $\mathbf{d}_j = \Psi d_j$ of length N^t is dominated by zero (or near zero) elements, where Ψ is the corresponding transform used (e.g., the discrete Fourier transform), then the dynamic signal $d_j[\cdot]$ can be approximated/recovered by seeking an "optimal" recovered signal $\hat{d}_j[\cdot]$ that matches the intermittently measured data, i.e.,

$$\begin{aligned} &\text{find } \hat{d}_j = \Psi^{-1}\hat{\mathbf{d}}_j \text{ such that} \\ &\quad g_j = \Phi_j \Psi^{-1}\hat{\mathbf{d}}_j, \quad \text{with minimal} \|\hat{\mathbf{d}}_j\|_1, \end{aligned} \tag{18}$$

where Φ_j is as defined in Eq. (17) (more details of the CS-based recovery is provided later). It has been shown [12], [27] that the solution to the above ℓ_1 optimization problem requires that the sensing matrix Φ_j satisfies a restricted isometry property (RIP) [21], [28]. In practice, this RIP property can be satisfied by choosing the sensing matrix Φ_j to be a random matrix (e.g., a Gaussian random matrix) [12], [29], i.e., the column index of all the non-zero elements in Ψ_j are randomly distributed over the entire range [12], [29]. Such a randomness requirements implies that the elements in the sequence $\mathbf{V}_{S_j}$, i.e., the measurement intervals at each POI ℓ_j, need to be randomly chosen from the total measurement interval set $\mathbf{S}_{tot}$.

The issue of spatial-temporal coupling in mobile sensing of dynamics, however, must be accounted in this random sampling. Specifically, random sampling (at all POIs) can result in the same measurement interval be assigned to multiple POIs, i.e., $\exists\ i,\ j \in \mathbf{S}_{tot},\ i \neq j$, such that

$$\langle \mathbf{e}_{N^t}(\mathbf{V}_{\mathbf{S}_i}), \mathbf{e}_{N^t}(\mathbf{V}_{\mathbf{S}_j}) \rangle \neq 0. \tag{19}$$

Moreover, the transition time can be too short for the transition required, i.e., $\exists\ p$ a POI-transition initialization interval (as in Definition 9) such that

$$\mathbf{Tr}_{p,q} < \mathbf{Tr}_{\ell_i,\ell_j}, \tag{20}$$

where $\mathbf{Tr}_{p,q}$ is as defined in Eq. (15), $p \in \mathbf{S}_i$ of POI ℓ_i and $q \in \mathbf{S}_j$ of POI ℓ_j, and $\mathbf{Tr}_{\ell_i,\ell_j}$ is defined in Eq. (3), respectively. Finally, the cost function Eq. (13) shall be minimized under the randomness requirement too. Thus, the temporal-spatial coupling, the POI-transition constraint, and the optimization of the mapping strategy must be accounted for.

III. Optimal Single Mobile Sensing of a Dynamic Field

We propose to extend the CS technique to solve the OSMS-DF problem. The idea is to remove the temporal-spatial coupling through a partition-pairing process, account for the POI-transition constraint through a check-and-removal process, and optimize the measurement decision through a shuffle-and-pairing process based on the simulated annealing algorithm.

A. Proposed algorithm

First, elements in the total measurement set $\mathbf{S}_{tot}$ are randomly permuted by following a uniform distribution [30], and

This article has been accepted for publication in a future issue of this journal, but has not been fully edited. Content may change prior to final publication. Citation information: DOI 10.1109/TMC.2021.3125201, IEEE Transactions on Mobile Computing

partitioned into N^s number of sub-measurement sets, $\mathbf{S}_j$, for $j = 1, 2, \cdots, N^s$,

$$\begin{aligned} &\mathbf{S}_j = \text{Random}\left(\mathbf{S}^c_{j-1}, U(1, |\mathbf{S}^c_{j-1}|), N^\ell_j\right), \text{ with} \\ &\mathbf{S}^c_j = \mathbf{S}^c_{j-1} \setminus \mathbf{S}_j, \text{ and } \mathbf{S}^c_0 = \mathbf{S}_{tot}, \end{aligned} \tag{21}$$

where, respectively, "Random$(S, D(1, |S|), N_d)$" denotes the operation of randomly selecting N_d number of elements from set S ($N_d \leq |S|$) according to the distribution, $D(1, |S|)$, $U(1, N)$ denotes one-dimensional uniform distribution of N elements, and $S_1 \setminus S_2$ denotes the set complement operation, i.e., $S^c_2 = S_1 \setminus S_2$ is the complement of S_2 in S_1 for $S_2 \subset S_1$.

Next, the sequences of the obtained sub-measurement sets $\mathbf{S}_j$s, $\mathbf{V}_{\mathbf{S}_j}$s, are assigned to each POI ℓ_j respectively, i.e., $\mathbf{V}_{\mathbf{S}_j} \to \ell_j$, resulting in the so-called *preliminary measurement decision* (PMD) $\mathbb{M}^P$

$$\mathbb{M}^P = \begin{bmatrix} \mathbf{e}_{N^t}(\mathbf{V}_{\mathbf{S}_1}) \\ \mathbf{e}_{N^t}(\mathbf{V}_{\mathbf{S}_2}) \\ \vdots \\ \mathbf{e}_{N^t}(\mathbf{V}_{\mathbf{S}_{N^s}}) \end{bmatrix}_{N^s \times N^t}, \tag{22}$$

where $\mathbf{S}_\mathcal{T} = \emptyset$—the agent mobility constraint has not yet been considered, and thereby, is not satisfied in general.

We propose a check-and-removal process to update the PMD $\mathbb{M}^P$. Also in the PMD $\mathbb{M}^P$, for any $p \in \mathbf{S}_i$ ($p = 1, 2, \cdots, N^t$) being a transition-initialization interval, the corresponding q^{th} interval (see Definition 9) equals to $p+1$, and the between-POI transition can be checked via Eq. (20) and adjusted by assigning more intervals for transition. Thus,

$$\begin{aligned} &\text{For } p \in \mathbf{S}_i \text{ a transition-initialization interval,} \\ &\quad \text{if Eq. (20) occurs, then find the smallest } \hat{q} \geq p+2 \text{ in} \\ &\quad \text{some } \mathbf{S}_k \text{ of the POI } \ell_k, \text{ such that} \\ &\qquad \mathbf{Tr}_{p,\hat{q}} \geq \mathbf{Tr}_{\ell_i,\ell_k}, \text{ and } \hat{q} - p > 1, \\ &\quad \text{then if } k = i \\ &\qquad \mathbf{S}^r_i = \{\mathbf{S}^r_i,\ p+1, \cdots,\ \hat{q}-1\}, \\ &\quad \text{otherwise} \\ &\qquad \mathbf{S}_\mathcal{T} = \{\mathbf{S}_\mathcal{T},\ p+1, \cdots,\ \hat{q}-1\}, \end{aligned} \tag{23}$$

where $\mathbf{S}^r_i$ is called the i^{th} reservoir measurement set, and $\mathbf{S}_\mathcal{T} = \emptyset$, and $\mathbf{S}^r_i = \emptyset$ initially. Thus with this check-and-removal process, additional transition time is added only when the before- and after- transition POIs are different, otherwise that transition is eliminated and additional measurements are taken at the before-transition POI. Afterwards, the PMD $\mathbb{M}^P$ is updated accordingly to obtain the following *feasible measurement decision* (FMD), $\mathbb{M}^F$,

$$\mathbb{M}^F = \begin{bmatrix} \mathbf{e}_{N^t}(\mathbf{V}_{\mathbf{S}_1 \setminus \mathbf{S}_\mathcal{T}}) \\ \mathbf{e}_{N^t}(\mathbf{V}_{\mathbf{S}_2 \setminus \mathbf{S}_\mathcal{T}}) \\ \vdots \\ \mathbf{e}_{N^t}(\mathbf{V}_{\mathbf{S}_{N^s} \setminus \mathbf{S}_\mathcal{T}}) \end{bmatrix}_{N^s \times N^t}. \tag{24}$$

The computation complexity of this check-and-removal process is $\mathcal{O}(N^t)$.

The FMD $\mathbb{M}^F$, however, may not be optimal to minimize the total transition distance and the total transition time, i.e., not optimal to minimize the cost function J in Eq. (13). As the POIs are known a priori, and through the above check-and-removal process, both the number of transitions and the corresponding POIs are known, so are the total transition distance L_{tot} and the total time spent on the transition $|\mathbf{S}_\mathcal{T}|$.

This optimization problem of Eq. (13) is non-deterministic polynomial-time hard (NP-hard)—as in the traveling salesman problem (TSP) [31]. Thus, we propose to seek a sub-optimal solution through a simulated annealing (SA) [22] based shuffle-and-pair process. The basic idea of SA is to combine the gradient decent search (i.e., search in the cost-decreasing direction) with random jumps to avoid being trapped into local minimum (i.e., by searching in the cost-increasing direction instead) during the iterative searching process. The random jumps are regulated through a factor called temperature T^{SA} via an exponential function $e^{C\Delta J/T^{SA}}$ (mimics the physical annealing process) [22].

First, an initial FMD $\mathbb{M}^F_0$ is obtained via the check-and-removal process from an initial PDM $\mathbb{M}^P_0$, and the corresponding cost function J_0 for $\mathbb{M}^F_0$ is calculated via Eq. (13). Then, in each i^{th} iteration of the SA process, both the PMD $\mathbb{M}^P_{i-1}$ and the FMD $\mathbb{M}^F_{i-1}$ (for $i \geqslant 1$) are used in the shuffle-and-pair process to obtain the next PMD $\mathbb{M}^P_i$ and update the FMD towards the optimal: In the current PMD $\mathbb{M}^P_{i-1}$, a small number of N^f elements ($N^f \ll N^\ell_j$, N^ℓ_j: total number of measurement intervals at each j^{th} POI) is randomly selected (via uniform distribution) from each j^{th} sub-measurement set in the i^{th} iteration, $\mathbf{S}_{j,i}$, to form the sub-shuffle set, $\tilde{\mathbf{S}}_{j,i}$ for $j = 1, \cdots, N^s$, and then combined together to form the interval-shuffle set $\tilde{\mathbf{S}}_i$ (for the i^{th} iteration)

$$\begin{aligned} &\tilde{\mathbf{S}}_i = \bigcup_{j=1}^{N^s} \tilde{\mathbf{S}}_{j,i}, \quad \text{with} \\ &\tilde{\mathbf{S}}_{j,i} = \text{Random}(\mathbf{S}_{j,i}, U(1, |\mathbf{S}_{j,i}|), N^f). \end{aligned} \tag{25}$$

The obtained interval-shuffle set $\tilde{\mathbf{S}}_i$ is then randomly permuted and partitioned into N^s number of subsets each of size N^f (called the updated sub-shuffle sets), $\tilde{\mathbf{S}}^u_{j,i}$,

$$\begin{aligned} &\tilde{\mathbf{S}}^u_{j,i} = \text{Random}\left(\tilde{\mathbf{S}}^{u,c}_{j,i}, U(1, |\tilde{\mathbf{S}}^{u,c}_{j,i}|), N^f\right), \quad \text{with} \\ &\tilde{\mathbf{S}}^{u,c}_{j,i} = \tilde{\mathbf{S}}^{u,c}_{j-1,i} \setminus \tilde{\mathbf{S}}^u_{j,i}, \quad \text{with} \\ &\tilde{\mathbf{S}}^{u,c}_{0,i} = \tilde{\mathbf{S}}_i \text{ initially.} \end{aligned} \tag{26}$$

Next, each updated sub-shuffle set $\tilde{\mathbf{S}}^u_{j,i}$ is paired with the complement of the sub-shuffle set in the corresponding sub-measurement set, $\mathbf{S}_{j,i} \setminus \tilde{\mathbf{S}}_{j,i}$, to obtain the updated sub-measurement set $\bar{\mathbf{S}}_{j,i}$,

$$\bar{\mathbf{S}}_{j,i} = \tilde{\mathbf{S}}^u_{j,i} \cup \left(\mathbf{S}_{j,i} \setminus \tilde{\mathbf{S}}_{j,i}\right), \tag{27}$$

and then the next PMD $\mathbb{M}^P_i$,

$$\mathbb{M}^P_i = \begin{bmatrix} \mathbf{e}_{N^t}(\mathbf{V}_{\bar{\mathbf{S}}_{1,i}}) \\ \mathbf{e}_{N^t}(\mathbf{V}_{\bar{\mathbf{S}}_{2,i}}) \\ \vdots \\ \mathbf{e}_{N^t}(\mathbf{V}_{\bar{\mathbf{S}}_{N^s,i}}) \end{bmatrix}_{N^s \times N^t}, \tag{28}$$

This article has been accepted for publication in a future issue of this journal, but has not been fully edited. Content may change prior to final publication. Citation information: DOI 10.1109/TMC.2021.3125201, IEEE Transactions on Mobile Computing

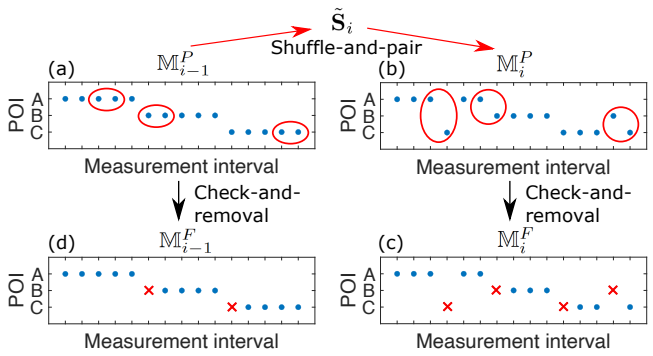

Fig. 2: A schematic representation of the FMD updating process in the SA-based shuffle-and-pair process for three POI case (denoted as "A", "B", and "C" in the y-axis label): (a) sub-shuffle sets $\tilde{\mathbf{S}}_{j,i}$s (those in the red circles) are randomly selected from the i^{th} PMD $\mathbb{M}_{i-1}^P$ and grouped together to form the interval-shuffle set $\tilde{\mathbf{S}}_i$, then (b) $\tilde{\mathbf{S}}_i$ is repartitioned into N^s number of subsets and each subset is paired with the updated sub-shuffle sets $\tilde{\mathbf{S}}_{j,i}^u$ (those in red circles) and assigned to the POIs to form the next PMD $\mathbb{M}_i^P$; (c) The new FMD $\mathbb{M}_i^F$ is generated via the check-and-removal process from the PMD $\mathbb{M}_i^P$ (where the red-crosses denote the removed intervals), and (d) the FMD obtained from the previous PMD $\mathbb{M}_{i-1}^P$ via the check-and-removal process directly (without the shuffle-and-pair process in (b) and (c)) is also obtained as $\mathbb{M}_{i-1}^F$, for comparison in the SA updating.

where each $\mathbf{V}_{\bar{\mathbf{S}}_{j,i}}$ is the sequence corresponding to each set $\bar{\mathbf{S}}_{j,i}$, respectively. Then the check-and-removal process (see Eq. (23)) is applied to $\mathbb{M}_i^P$ to obtain the corresponding FMD $\mathbb{M}_i^F$. This shuffle-and-pair process of the PMD is depicted in Fig. 2.

The cost function corresponding to the FMD $\mathbb{M}_i^F$, J_i, will be compared to that of the previous iteration J_{i-1}: 1) If the difference $\Delta J_i = J_i - J_{i-1} \leq 0$, this FMD $\mathbb{M}_i^F$ will be accepted; 2) Otherwise, the FMD $\mathbb{M}_i^F$ will be accepted with a probability $P_i = e^{-C\Delta J_i/T_i^{SA}}$, i.e., $\mathbb{M}_i^F$ will be accepted if $P_i > \rho$, with ρ a random number generated via the uniform distribution over the interval $(0,\ 1)$, $C > 0$ a pre-chosen constant, and $T_i^{SA} > 0$ the annealing "temperature", respectively; Otherwise (i.e., $P_i \leq \rho$), the previous PMD and FMD, $\mathbb{M}_{i-1}^P$ and $\mathbb{M}_{i-1}^F$, respectively, are inherited as the current PMD $\mathbb{M}_i^P$ and FMD $\mathbb{M}_i^F$, respectively, i.e., $\mathbb{M}_i^P = \mathbb{M}_{i-1}^P$ and $\mathbb{M}_i^F = \mathbb{M}_{i-1}^F$. Then, the annealing temperature T^{SA} is decreased by following an a priori chosen annealing schedule, e.g., set $T_{i+1}^{SA} = \delta \cdot T_i^{SA}$ with a pre-chosen $\delta \in (0, 1)$ and initial value $T_1^{SA} > 0$, and the above updating process is repeated until the annealing index T^{SA} is less than a preset threshold $T_{\min}^{SA}$.

The efficiency vs. the optimization quality of the above SA-based searching process can be traded-off through the parameters involved: The optimization quality can be improved with more iterations by choosing a large initial temperature T_1^{SA}, a large iteration-update parameter δ (close to 1), and a small threshold parameter C in the probability of each iteration $P_i = e^{-C\Delta J_i/T_i^{SA}}$, and vise versa. This optimization process is summarized in Alg. 1.

Algorithm 1: SA-based Optimization of the FMD

Input: PMD $\mathbb{M}_0^P$, FMD $\mathbb{M}_0^F$
Output: Optimal FMD $\mathbb{M}^{F*}$

Initialization: annealing index T_1^{SA}, threshold $T_{\min}^{SA}$, constant C, δ, the cost function J_0 of the FMD $\mathbb{M}_0^F$;
while $T_i^{SA} > T_{\min}^{SA}$ **do**
  Generate a new PMD $\mathbb{M}_i^P$ in the neighbor of current PMD $\mathbb{M}_{i-1}^P$ by the shuffle-and-pair process;
  Generate the corresponding FMD $\mathbb{M}_i^F$ of PMD $\mathbb{M}_i^P$ by check-and-removal;
  Compute the cost function J_i of the new FMD $\mathbb{M}_i^F$;
  if $\Delta J_i = J_i - J_{i-1} \leq 0$ **then**
    accept $\mathbb{M}_i^F$ and $\mathbb{M}_i^P$;
  else
    accept $\mathbb{M}_i^F$ and $\mathbb{M}_i^P$ with probability $P = e^{-\frac{C\Delta J}{T_i^{SA}}}$;
  Reduce the annealing index T^{SA} by an annealing schedule $T_{i+1}^{SA} = \delta \cdot T_i^{SA}$;
Set the optimal FMD $\mathbb{M}^{F*} = \mathbb{M}_i^F$;

During the mobile sensing process, the optimal MD $\mathbb{M}^{F*}$ obtained above is executed by the agent R to capture the dynamic signals at all POIs, and the intermittently measured data at each j^{th} POI, ℓ_j for $j = 1, 2, \cdots, N^s$, are acquired and used to recover/approximate the corresponding dynamic signal—by solving Eq. (12) via the compressed sensing technique in time domain.

B. Recovery via Compressed Sensing

For completeness, we briefly describe below the implementation of the compressed sensing technique in the proposed OSMS-DF approach. For any given POI ℓ_j, the data measured at the N_j^ℓ number of measurement intervals, $g_j[p]$ for $p = 1, 2, \cdots, N_j^\ell$, is utilized to recover/approximate the dynamic signal over the total N^t sampling periods, $d_j[q]$ for $q = 1, 2, \cdots, N^t$. First, the measured data $g_j[\cdot]$ is transformed to a sparse domain through an appropriately chosen transform, for example, the discrete cosine transform (DCT) on $g_j[\cdot]$,

$$\eta(k) = \sqrt{\frac{2}{N_j^\ell}} \sum_{p=1}^{N_j^\ell} g_j[p] \frac{1}{\sqrt{1+\delta_{p1}}} \cos\left(\frac{\pi}{2N_j^\ell}(p-1)(2k-1)\right), \quad \text{for } p = 1, \cdots, N_j^\ell, \text{ and } k = 1, 2, \cdots, N_j^\ell, \tag{29}$$

where N_j^ℓ, δ_{p1}, and η denote the length of the transformed signal of $g_j[p]$, the Kronecker delta, and the sparse representation of the observation vector $g_j[p]$ in the transformed domain, respectively. Then, the dynamic signal on each j^{th} POIs, $d_j[\cdot]$, for $j = 1, 2, \cdots, N^s$, is recovered by minimizing the ℓ_1 norm

This article has been accepted for publication in a future issue of this journal, but has not been fully edited. Content may change prior to final publication. Citation information: DOI 10.1109/TMC.2021.3125201, IEEE Transactions on Mobile Computing

of the approximated signal in the transformed domain, $\hat{\mathbf{d}}_j$, [12], [32], i.e.,

$$\begin{aligned} &\text{minimize} \quad \|\hat{\mathbf{d}}_j\|_1 \\ &\text{subject to} \quad g_j = \Phi_j \hat{d}_j = \Phi_j \Psi^{-1} \hat{\mathbf{d}}_j \end{aligned} \tag{30}$$

with

$$\|\hat{\mathbf{d}}_j\|_1 := \sum_{q=1}^{N^t} |\hat{\mathbf{d}}_j[q]|. \tag{31}$$

The above constrained ℓ_1 optimization problem can be readily solved by using existing algorithms (e.g., [32]).

Finally, the data measured during those intervals in the reservoir set $\mathbf{S}^r$, where $\mathbf{S}^r = \cup_{j=1}^{N_s} \mathbf{S}^r_j$, can be utilized to further improve the accuracy. For example, when the compressed ratio is relatively high and the recovery quality can be further enhanced by having more sampling data, then these data can be combined with those acquired in $\mathbf{S}_j$, and then used in the CS-based recovery above. Alternatively, these data can be used to replace those recovered for the intervals in $\mathbf{S}^r_j$. More advanced techniques such as nonlinear interpolation [33] can be explored to further exploit the data acquired in the reservoir set.

The proposed OSMS-DF technique is summarized in Alg. 2.

Algorithm 2: Optimal Single Mobile Sensing of Dynamic Field (OSMS-DF)

Input: total measurement time $\mathbf{T}^{tot}$, POIs $\mathcal{L}_s$, agent maximum transition speed $v_{\max}$

Output: Dynamic signals at each POI

1 Initialization: Discretization ($\mathbf{T}^{tot} \sim \mathbf{V}_{\mathbf{S}_{tot}}$, pre-calculation (all $|\ell_i - \ell_j|/v_{\max}$);

2 Randomly partition the total measurement set $\mathbf{S}_{tot}$ into N^s number of sub-measurement sets $\mathbf{S}_i$ for $i = 1, 2, \cdots, N^s$, and assign the corresponding sequence $\mathbf{V}_{\mathbf{S}_i}$s to POI ℓ_i, respectively, to generate PMD $\mathbb{M}^P$;

3 Check agent mobility constraint and move those unsatisfying POI-transition intervals to the transition set $\mathbf{S}_\mathcal{T}$ to generate the FMD $\mathbb{M}^F$;

4 Use the PMD $\mathbb{M}^P$ and the FMD $\mathbb{M}^F$ obtained above as the input in the simulated annealing process to obtain the optimal FMD $\mathbb{M}^{F*}$ (see Alg. 1);

5 Conduct the mobile sensing according to the optimal FMD $\mathbb{M}^{F*}$;

6 Recover the dynamic signal at each POI via the compressed sensing.

IV. Analysis of the Proposed OSMS-DF Process

As the total transition time, i.e., the number of intervals in the transition set $\mathbf{S}_\mathcal{T}$, $|\mathbf{S}_\mathcal{T}|$, directly effects the recovery/approximation quality, i.e., the smaller is $|\mathbf{S}_\mathcal{T}|$, the larger amount of time is used for the measurement, we characterize, in the proposed OSMS-DF approach, how the number of measurement intervals at each POI varies in the probability sense—The randomness nature of the SA process and the distribution of the measurement intervals imply that the assignment of an interval to measurement at a POI or to a POI-transition is also random.

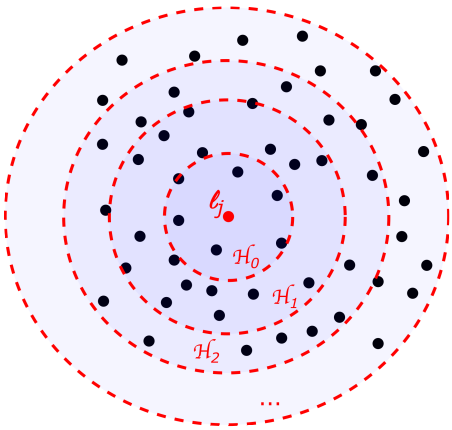

Fig. 3: A schematic representation of neighborhoods at different level, $\mathcal{H}_0, \mathcal{H}_1, \mathcal{H}_2, \cdots$ of a POI ℓ_j: the black dots denote the POIs other than ℓ_j, the red-dashed circles denote the boundaries of each $\mathcal{H}_k$ neighborhood, and the area inside each red dashed circle denote the corresponding neighborhood $\mathcal{H}_0, \mathcal{H}_1, \mathcal{H}_2, \cdots$, respectively.

Particularly, for any given POI ℓ_j, all other POIs, ℓ_is for $i = 1, 2, \cdots, N^s$ and $i \neq j$, can be grouped into neighborhoods of different levels based on the POI-transition time needed, $\mathcal{H}_k$, $k = 0, 1, \cdots, N^{tr}_{\max}$, where the level of neighborhood is determined by the discretized transition time needed: $\ell_i \in k^{th}$-level neighborhood $\mathcal{H}_k$ of ℓ_j if agent R can be transited from ℓ_i to ℓ_j by having additional k number of measurement intervals (see Fig. 3), i.e.,

$$\begin{aligned} \ell_i \in \mathcal{H}_k, \quad \text{if} \quad D_{tr}(\mathbf{Tr}^*_{\ell_i,\ell_j}) \leq k, \quad \text{and} \\ \mathcal{H}_0 \subset \mathcal{H}_1 \subset \mathcal{H}_2 \cdots \subset \mathcal{H}_{N^{tr}_{\max}}, \end{aligned} \tag{32}$$

where, respectively, $\mathbf{Tr}^*_{\ell_i,\ell_j}$ is as defined in Eq. (20), $D_{tr}(\cdot)$ is given in Eq. (8), and $N^{tr}_{\max}$ is as given in Eq. (9)—by Assumption 7, when $k = N^{tr}_{\max}$, the k^{th}-level neighborhood $\mathcal{H}_k$ contains all the POIs, i.e., $\mathcal{H}_{N^{tr}_{\max}} = \mathcal{L}_s$. Each of the k^{th} neighborhood of ℓ_j is a closed set.

The Lemma below quantifies the probability of any given p^{th} measurement interval being assigned to a POI ℓ_j, $P_{\ell_j,p}$.

Lemma 10. *Let Assumptions 1, 6, and 7 hold, then in the proposed OSMS-DF method, the probability of agent R measuring at any given j^{th} POI ℓ_j ($j = 1, 2, \cdots, N^s$) in any given p^{th} interval ($p = 2, \cdots, N^t$), $P_{\ell_j,p}$, is given by*

$$\begin{aligned} P_{\ell_j,p} = P_{\ell_j,1} \Bigg[\sum_{\ell_i \in \mathcal{H}_0} P_{\ell_i,p-1} + \sum_{k=1}^{\min(p-2, N^{tr}_{\max}-1)} \Bigg(\\ \Big(\prod_{\tau=1}^{k} P^{\mathbf{Tr},r}_{p-\tau} \Big) \cdot \Big(\sum_{\ell_i \in \mathcal{H}_k} P_{\ell_i,p-k-1} \Big) \Bigg) \\ + \prod_{\tau=1}^{\min(p-1, N^{tr}_{\max})} P^{\mathbf{Tr},r}_{p-\tau} \Bigg] \end{aligned} \tag{33}$$

$$P_p^{\mathbf{Tr},r} = 1 - \sum_{\ell_i \in \mathcal{L}_s} P_{\ell_i,p}, \tag{34}$$

where $P_{\ell_j,1}$ is the probability to choose POI ℓ_j initially (i.e., the probability of choosing POI ℓ_j at the beginning of the entire measurement process), and $P_p^{\mathbf{Tr},r}$ is the probability for moving the p^{th} measurement interval to the reservoir set $\mathbf{S}^r$ or to the transition set $\mathbf{S}_\mathcal{T}$ by the check-and-removal process, respectively.

Proof. We show Eq. (33) first. For a given FMD $\mathbb{M}^F$, consider the general scenario where in the current $(p-1)^{th}$ measurement interval, agent R is at a given POI ℓ_i, and the next measurement POI ℓ_j is in the k^{th}-level neighborhood of ℓ_i, i.e., $\ell_j \in \mathcal{H}_k$ for $k = 0, \cdots, N_{\max}^{tr}$. Thus, the probability of taking measurement at POI ℓ_j in the next p^{th} interval, $P_{\ell_j,\ell_i,p}$, is the sum of the probability of the following two cases: Case 1: $\ell_j \in \mathcal{H}_0$ (including $\ell_j = \ell_i$), $P_{\ell_j,\ell_i,p}^{\mathcal{H}_0}$; and Case 2: $\ell_j \in \mathcal{H}_k$ for $k > 0$, $P_{\ell_j,\ell_i,p}^{\mathcal{H}_k}$,

$$P_{\ell_j,\ell_i,p} = P_{\ell_j,\ell_i,p}^{\mathcal{H}_0} + P_{\ell_j,\ell_i,p}^{\mathcal{H}_k}. \tag{35}$$

In Case 1, no additional transition time is needed (i.e., the transition can be attained within the minimal transition time I^T), thus the probability $P_{\ell_j,\ell_i,p}^{\mathcal{H}_0}$ equals to that of having agent R at POI ℓ_i in the $(p-1)^{th}$ interval, $P_{\ell_i,p-1}$, i.e.,

$$P_{\ell_j,\ell_i,p}^{\mathcal{H}_0} = P_{\ell_i,p-1}. \tag{36}$$

In Case 2, agent R is able to measure at POI ℓ_j only if it can be transited from POI ℓ_i to POI ℓ_j within the given transition time, i.e., only if Eq. (32) holds at the p^{th} interval. This condition requires that $p > k+1$ and all the preceding k consecutive number of intervals, $p-1, p-2, \cdots, p-k$, are all assigned for the POI-transition from ℓ_i to ℓ_j. Thus, the probability $P_{\ell_j,\ell_i,p}^{\mathcal{H}_k}$ is given by the joint probability of having all $p-k, p-(k-1), \cdots, p-1 \in \mathbf{S}_\mathcal{T}$, $\prod_{\tau=1}^{k} P_{p-\tau}^{\mathbf{Tr},r}$, and having agent R at POI ℓ_i in the $(p-k-1)^{th}$ interval, $P_{\ell_i,p-k-1}$, i.e.,

$$P_{\ell_j,\ell_i,p}^{\mathcal{H}_k} = \left(\prod_{\tau=1}^{k} P_{p-\tau}^{\mathbf{Tr},r} \right) \cdot P_{\ell_i,p-k-1}, \quad \text{for } p > k+1. \tag{37}$$

As the transited-to POI ℓ_j can be any one of the POIs in the $\mathcal{H}_k$ neighborhood of ℓ_i, i.e., the probability of choosing ℓ_j among all the POIs in the $\mathcal{H}_k$ neighborhood is the same as that of choosing ℓ_j without the POI-transition time constraint, or equivalently, the initial probability of choosing ℓ_j among all POIs, $P_{\ell_j,1}$, the probability of measuring at any POI ℓ_j in the p^{th} interval, $\hat{P}_{\ell_j,\ell_i,p}$, can be obtained via Eqs. (35,36,37) as

$$\begin{aligned} \hat{P}_{\ell_j,\ell_i,p} &= P_{\ell_j,1} P_{\ell_j,\ell_i,p} \\ &= P_{\ell_j,1} \left(P_{\ell_j,\ell_i,p}^{\mathcal{H}_0} + P_{\ell_j,\ell_i,p}^{\mathcal{H}_k} \right) \\ &= P_{\ell_j,1} \Bigg(P_{\ell_i,p-1} \\ &\quad + \left(\left(\prod_{\tau=1}^{k} P_{p-\tau}^{\mathbf{Tr},r} \right) \cdot \left(P_{\ell_i,p-k-1} \right) \right) \Bigg). \end{aligned} \tag{38}$$

Similarly, as the transited-from POI ℓ_i can be any one of those in the $\mathcal{H}_0$ level (case 1) or any of those in the $\mathcal{H}_k$ level (case 2) neighborhood of ℓ_j, the probability of measuring at any given POI ℓ_j in the p^{th} interval can be obtained from Eq. (38) as

$$\begin{aligned} \hat{P}_{\ell_j,p} = P_{\ell_j,1} \Bigg[& \sum_{\ell_i \in \mathcal{H}_0} P_{\ell_i,p-1} \\ & + \left(\prod_{\tau=1}^{k} P_{p-\tau}^{\mathbf{Tr},r} \right) \cdot \left(\sum_{\ell_i \in \mathcal{H}_k} P_{\ell_i,p-k-1} \right) \Bigg]. \end{aligned} \tag{39}$$

Finally, as in general, the level of neighborhood that shall be considered increases with the interval p until the maximum level $k = N_{\max}^{tr}$ is reached, the number of neighborhood $\mathcal{H}_k$ at most equals to $N_{\max}^{tr}$, the probability of measuring at any given POI ℓ_j in the p^{th} interval is given by

$$\begin{aligned} P_{\ell_j,p} &= \sum_{\ell_i \in \mathcal{L}_s} \hat{P}_{\ell_j,p} \\ &= P_{\ell_j,1} \Bigg[\sum_{\ell_i \in \mathcal{H}_0} P_{\ell_i,p-1} + \sum_{k=1}^{\min(p-2, N_{\max}^{tr}-1)} \Bigg(\\ &\quad \left(\prod_{\tau=1}^{k} P_{p-\tau}^{\mathbf{Tr},r} \right) \cdot \left(\sum_{\ell_i \in \mathcal{H}_k} P_{\ell_i,p-k-1} \right) \Bigg) \\ &\quad + \prod_{\tau=1}^{\min(p-1, N_{\max}^{tr})} P_{p-\tau}^{\mathbf{Tr},r} \Bigg]. \end{aligned} \tag{40}$$

The last term in Eq. (40) is the probability of having agent R in the highest possible level of neighborhood of ℓ_j in the previous $(p - (\min(p-1,\ N_{\max}^{tr})))^{th}$ interval. With the above probability quantified, the probability of moving any p^{th} interval to the reservoir set $\mathbf{S}^r$ or to the transition set $\mathbf{S}_\mathcal{T}$ by the check-and-removal process can be obtained directly as that of the interval not assigned for measurement at any POI, as given in Eq. (34). This completes the proof. □

Lemma 10 shows that the probability of measuring at a given POI depends on the index of the measurement interval p itself. Next, we examine as the measurement interval index p increases along with the total number of measurement intervals N^t, how the probability of measuring at any given POI varies, i.e., how the following distribution vector $\mathbf{P}_p$ varies,

$$\mathbf{P}_p = \left[P_{\ell_1,p}, P_{\ell_2,p}, \cdots, P_{\ell_{N^s},p} \right]^T. \tag{41}$$

We show the asymptotic convergence of this distribution for the case where the POI-transition can be attained within one measurement interval, $N_{\max}^{tr} = 1$.

Theorem 11. *Let Assumptions 1, 6, and 7 hold, and for any given j^{th} POI ℓ_j, all other POIs are in the $\mathcal{H}_0$ or $\mathcal{H}_1$ neighborhood of ℓ_j, then in the proposed OSMS-DF method, the measurement distribution vector $\mathbf{P}_p$ in Eq.* (41) *converges as the index p increases with the total number of measurement intervals N^t, i.e.,*

$$\lim_{p \to N^t, N^t \to \infty} (\mathbf{P}_p - \mathbf{P}_{p-1}) = \vec{\mathbf{0}}, \tag{42}$$

where $\vec{\mathbf{0}} \in \Re^{N^s \times 1}$ denotes a zero vector.

Proof. We proceed by defining a weight vector $\mathbf{W}_{\mathcal{H}_k}^{\ell_j} \in \Re^{N^s \times 1}$ where $\mathbf{W}_{\mathcal{H}_k}^{\ell_j}[i] = 1$ if POI $\ell_i \in \mathcal{H}_k$ of ℓ_j and

This article has been accepted for publication in a future issue of this journal, but has not been fully edited. Content may change prior to final publication. Citation information: DOI 10.1109/TMC.2021.3125201, IEEE Transactions on Mobile Computing

$\mathbf{W}^{\ell_j}_{\mathcal{H}_k}[i] = 0$ otherwise, and rewriting Eq. (33) in vector inner product form by using $\mathbf{W}^{\ell_j}_{\mathcal{H}_k}$ and the definition in Eq. (41) as

$$\begin{aligned} P_{\ell_j,p} = P_{\ell_j,1}\Bigg[&\langle \mathbf{W}^{\ell_j}_{\mathcal{H}_0}, \mathbf{P}_{p-1}\rangle \\ &+ \sum_{k=1}^{\min(p-2,N^{tr}_{\max}-1)} \Big(\prod_{\tau=1}^{k} P^{\mathbf{Tr},r}_{p-\tau}\Big)\langle \mathbf{W}^{\ell_j}_{\mathcal{H}_k}, \mathbf{P}_{p-k-1}\rangle \\ &+ \prod_{\tau=1}^{\min(p-1,N^{tr}_{\max})} P^{\mathbf{Tr},r}_{p-\tau}\Bigg]. \end{aligned} \tag{43}$$

For case $N^{tr}_{\max} = 0$, i.e., all the POIs are in the $\mathcal{H}_0$-level neighborhood of ℓ_j, no additional measurement interval is needed for the POI-transition, and $\mathbf{S}_{\mathcal{T}} = \emptyset$, thereby, $P^{\mathbf{Tr},r}_{p} = 0$ for any $p = 1, \cdots, N^t$, and Eq. (43) is simplified as

$$P_{\ell_j,p} = P_{\ell_j,1}\langle \mathbf{W}^{\ell_j}_{\mathcal{H}_0}, \mathbf{P}_{p-1}\rangle, \tag{44}$$

with $\mathbf{W}^{\ell_j}_{\mathcal{H}_0}[i] = 1$ for $i = 1, 2, \cdots, N^s$. As $\sum_{j=1}^{N^s} P_{\ell_j,p} = 1$, we have $P_{\ell_j,p} = P_{\ell_j,1}$ holds for any $p > 1$.

For case $N^{tr}_{\max} = 1$, all the POI-transition can be attained within at most one measurement period, i.e., all the POIs are in the neighborhood $\mathcal{H}_0$ or $\mathcal{H}_1$ of POI ℓ_j, Eq. (43) is simplified as

$$\begin{aligned} P_{\ell_j,p} &= P_{\ell_j,1}\left(\sum_{\ell_i\in\mathcal{H}_0} P_{\ell_i,p-1} + P_{\mathbf{Tr},p-1}\right) \\ &= P_{\ell_j,1}\left(\sum_{\ell_i\in\mathcal{H}_0} P_{\ell_i,p-1} + 1 - \sum_{\ell_i\in\mathcal{L}_s} P_{\ell_i,p-1}\right) \\ &= P_{\ell_j,1}\left(1 - \sum_{\ell_i\in\mathcal{L}_s\setminus\mathcal{H}_0} P_{\ell_i,p-1}\right) \\ &= -P_{\ell_j,1}\langle \mathbf{W}^{\ell_j}_{\mathcal{H}^-_0}, \mathbf{P}_{p-1}\rangle + P_{\ell_j,1}, \end{aligned} \tag{45}$$

where $\mathcal{H}^-_0 = \mathcal{L}_s \setminus \mathcal{H}_0$ is the complement set of $\mathcal{H}_0$ in set $\mathcal{L}_s$, and $\mathbf{W}^{\ell_j}_{\mathcal{H}^-_0}$ is the corresponding weight vector, i.e., $\mathbf{W}^{\ell_j}_{\mathcal{H}^-_0}[i] = 1$ if $\mathbf{W}^{\ell_j}_{\mathcal{H}_0}[i] = 0$ and $\mathbf{W}^{\ell_j}_{\mathcal{H}^-_0}[i] = 0$ otherwise.

By Eq. (45), the measurement distribution vector $\mathbf{P}_p$ can be obtained as

$$\mathbf{P}_p = -\widehat{\mathbf{W}}^T_{\mathcal{H}^-_0}\mathbf{P}_{p-1} + \mathbf{P}_1, \tag{46}$$

where $\widehat{\mathbf{W}}_{\mathcal{H}^-_0} \in \Re^{N^s\times N^s}$ is the weighting matrix given by

$$\widehat{\mathbf{W}}_{\mathcal{H}^-_0} = \left[P_{\ell_1,1}\mathbf{W}^{\ell_1}_{\mathcal{H}^-_0}, \cdots, P_{\ell_j,1}\mathbf{W}^{\ell_j}_{\mathcal{H}^-_0}, \cdots, P_{\ell_{N^s},1}\mathbf{W}^{\ell_{N^s}}_{\mathcal{H}^-_0}\right]. \tag{47}$$

As the diagonal elements of the above matrix $\widehat{\mathbf{W}}_{\mathcal{H}^-_0}$ are all zero (i.e., $\ell_j \in \mathcal{H}_0$ for $\forall j = 1, \cdots, N^s$), and $\sum_{j=1}^{N^s} P_{\ell_j,1} = 1$, the above matrix $\widehat{\mathbf{W}}_{\mathcal{H}^-_0}$ is a Markov matrix [34]. Hence, by the stability of Markov matrix [34], all the eigenvalues of $\widehat{\mathbf{W}}_{\mathcal{H}^-_0}$, λ_j, has $|\lambda_j| < 1$ for $j = 1, \cdots, N^s$, and the discrete dynamics system given by Eq. (46) is stable,

$$\lim_{p\to\infty}\mathbf{P}_p = \lim_{p\to\infty}\sum_{i=0}^{p-1}\left(-\widehat{\mathbf{W}}^T_{\mathcal{H}^-_0}\right)^i\mathbf{P}_1 \tag{48}$$

exists. This completes the proof. □

Remark 12. *The above result of Theorem 11 should also hold for higher-order case. By following similar algebraic operations it can be verified that in general scenario of $\mathcal{H}_k$-level neighborhood with $k \geq 2$, the distribution vector can also be represented by a difference dynamic equation as*

$$\widehat{\mathbf{P}}_p = \widehat{\mathbf{W}}\widehat{\mathbf{P}}_{p-1} + \widehat{\mathbf{P}}_1, \tag{49}$$

where

$$\widehat{\mathbf{P}}_p = \left[\mathbf{P}_p, \mathbf{P}_{p-1}, \cdots, \mathbf{P}_{p-N^{tr}_{\max}+1}\right]^T, \tag{50}$$

$$\widehat{\mathbf{P}}_1 = \left[\mathbf{P}_1, 0, \cdots, 0\right]^T, \tag{51}$$

are the augmented vectors of measurement period distribution, and

$$\widehat{\mathbf{W}} = \begin{bmatrix} -\widehat{\mathbf{W}}^T_{\mathcal{H}^-_0} & -\widehat{\mathbf{W}}^T_{\mathcal{H}^-_1} & \cdots & -\widehat{\mathbf{W}}^T_{\mathcal{H}^-_{N^{tr}_{\max}-2}} & -\widehat{\mathbf{W}}^T_{\mathcal{H}^-_{N^{tr}_{\max}-1}} \\ I & 0 & \cdots & 0 & 0 \\ 0 & I & \cdots & 0 & 0 \\ \vdots & \vdots & \ddots & \vdots & \vdots \\ 0 & 0 & \cdots & I & 0 \end{bmatrix} \tag{52}$$

is the corresponding discrete-dynamics matrix, with

$$\begin{aligned} \widehat{\mathbf{W}}_{\mathcal{H}^-_k} = \Big[&P_{\ell_1,1}\Big(\prod_{i=1}^{k} P^{\mathbf{Tr},r}_{p-i}\Big)\mathbf{W}^{\ell_1}_{\mathcal{H}^-_k}, \cdots, \\ &P_{\ell_j,1}\Big(\prod_{i=1}^{k} P^{\mathbf{Tr},r}_{p-i}\Big)\mathbf{W}^{\ell_j}_{\mathcal{H}^-_k}, \cdots, \\ &P_{\ell_{N^s},1}\Big(\prod_{i=1}^{k} P^{\mathbf{Tr},r}_{p-i}\Big)\mathbf{W}^{\ell_{N^s}}_{\mathcal{H}^-_k}\Big], \\ &\text{for } k = 1, \cdots, N^{tr}_{\max} - 1. \end{aligned} \tag{53}$$

Simulation has shown that the eigenvalues of $\widehat{\mathbf{W}}$ are always within the unit circle, and thereby, the distribution vector $\mathbf{P}_p$ alse converges. Rigorous proof of this extension will be pursued in the future work.

Remark 13. *Theorem 11 implies that the number of measurement intervals N^M_j at any POI ℓ_j can be estimated by the limit case—when the total number of measurement intervals N^t is large enough, the number of measurement intervals taken at any given POI ℓ_j, N^M_j, can be estimated as*

$$N^M_j = \frac{P_{\ell_j}}{P_{\ell_j,1}}N^\ell_j \approx \frac{P_{\ell_j,p}}{P_{\ell_j,1}}N^\ell_j, \tag{54}$$

where N^ℓ_j is the initial number of measurement intervals assigned to POI ℓ_j before the check-and-removal process, and P_{ℓ_j} can be estimated by the value of $P_{\ell_j,p}$ when the measurement index p is large enough.

Remark 14. *Theorem 11 also implies that the distribution of the measurement intervals between the POIs can be adjusted through the choice of initial distribution $\mathbf{P}_1$: Based on the transition requirements between the POIs (determined by the spatial distribution of the POIs relative to the agent mobility*

This article has been accepted for publication in a future issue of this journal, but has not been fully edited. Content may change prior to final publication. Citation information: DOI 10.1109/TMC.2021.3125201, IEEE Transactions on Mobile Computing

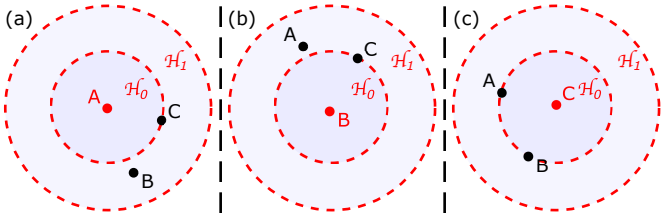

Fig. 4: A schematic representation of the neighborhoods of POIs A, B, and C, according to the preset agent speed limit (3 per transition interval) and the distances between these POIs in Table I, respectively.

capacity), the initial distribution can be selected such that the distribution of the measurement intervals can be adjusted towards chosen POIs over others (as demonstrated in the simulation example below). Such a non-uniform distribution of measurements is particularly useful when the POIs are largely dynamically heterogenous with respect to each other.

V. Simulation Example: Discrete Nanomechanical Mapping

In this section, we illustrate the proposed technique by applying it to discrete nanomechanical mapping (DNM) [24] of a heterogeneous sample in simulation.

A. Discrete Mapping of Dynamic Mechanical Variations at Nanoscale

In this simulation, we aim to quantify the nanomechanical variations of a heterogeneous polymer sample undergoing a temperature fluctuation—the scenario where the sample was putting on a heater whose temperature was controlled to follow a given profile. As such, the viscoelasticity of the sample would fluctuate along with the temperature fluctuation differently at different POIs. The proposed OSMS-DF technique was implemented to plan the measurement sequence of the cantilever probe between the chosen POIs (see Fig. 1), such that the dynamic viscoelasticity variations of the sample at these POIs can be recovered from the intermittently sampled data. For ease of comparison, the parameters had been normalized in the simulation.

More specifically, we consider three POIs A, B, and C, where the normalized distance between them are given in Table I, and the normalized maximum agent speed $v_{\max}$ was chosen as 3 (i.e., 3 unit distance per transition interval). The variations of the viscoelasticity at these three POIs under the effect of an external temperature profile $h_T(t)$ were modeled by the following linear Prony series [35]—by the time-temperature superposition principle of polymers [36]

$$E_i(h_T(t)) = E_{\infty,i} + \sum_{j=1}^{3} E_{i,j} \cdot \exp^{-h_T(t)/\tau_{i,j}}, \quad i = A, B, C \tag{55}$$

where $E_{\infty,i}$s, $E_{i,j}$s and $\tau_{i,j}$s, whose normalized values are given in Table II, are the fully relaxed modulus, the modulus coefficient, and the discrete relaxation times, respectively [36], and $h_T(t)$ was the external temperature field applied (i.e., the temperature of the polymer sample at time instant t).

To simplify the presentation and focus on the sensing performance itself, we assumed in the simulation that the viscoelasticity $E_i(h_T(t))$ was the measured signal—In AFM-based nanomechanical experiments, the viscoelasticity $E_i(t)$ is obtained by measuring the force applied and the indentation generated in the sample, and then computing $E_i(\cdot)$ from a chosen probe-sample interaction mechanics model (e.g., Hertzian Contact model) [35].

The temperature profile $h_T(\cdot)$ of a multiple sinusoidal signal was applied: $h_T(t) = 40 + 10\sin(0.04\pi t) + 10\sin(0.4\pi t) + 10\sin(4\pi t)$. The total measurement time was set at 120 seconds and the length of each measurement interval I^M was set at 0.1 second, with the ratio between the acquisition interval and the minimal transition interval at $I^A : I^T = 3 : 1$, resulting in a total of 1,200 measurement intervals. Thus, for the given distance between POI A and POI B in Table I, additional measurement interval was needed for POI A-B transition.

B. Implementation of the OSMS-DF Technique

The simulation was implemented in MATLAB. First, the total 1,200 measurement intervals were randomly permuted by following a uniform distribution, then partitioned into three sub-measurement sets $\mathbf{S}_k$ with $|\mathbf{S}_k| = 400$ for $k = 1, 2, 3$ (see Eq. (21)). Then, the corresponding sequence $\mathbf{V}_{\mathbf{S}_k}$s were assigned to each POI ℓ_j, respectively, $k = 1, 2, 3$ for $\ell_j = A, B, C$, respectively, resulting in an initial PMD $\mathbb{M}_0^P \in \Re^{3\times 1200}$ (see Eq. (22)). The proposed check-and-removal process was applied to this initial PMD $\mathbb{M}_0^P$, and the obtained FMD $\mathbb{M}_0^F$ was employed along with $\mathbb{M}_0^P$ as the initial choice in the SA-based shuffle-and-pair process to minimize the cost function Eq. (13), where the weights were chosen as $c_1 = 1$ and $c_2 = 20/9$ to equally weight the transition distance and the total measurement time (the value of c_2 equaled to the averaged transition distance). Ten out of 400 measurement periods were randomly selected (based

TABLE I: Distance between the sampling locations (POIs) A, B, and C with the maximum agent speed at 3 per transition interval and the neighborhood relations between them ($\mathcal{H}_0$ or $\mathcal{H}_1$).

distance, neighborhood	A	B	C
A	0, $\mathcal{H}_0$	4, $\mathcal{H}_1$	3, $\mathcal{H}_0$
B	4, $\mathcal{H}_1$	0, $\mathcal{H}_0$	3, $\mathcal{H}_0$
C	3, $\mathcal{H}_0$	3, $\mathcal{H}_0$	0, $\mathcal{H}_0$

TABLE II: The parameters of the Prony model at the three POIs.

POI	A	B	C
E_∞ (MPa)	5	5	5
E_1 (MPa)	1	1	1
E_2 (MPa)	3	2	1
E_3 (MPa)	5	3	1
τ_1 (ms)	10	50	100
τ_2 (ms)	1	10	50
τ_3 (ms)	0.1	1	10

This article has been accepted for publication in a future issue of this journal, but has not been fully edited. Content may change prior to final publication. Citation information: DOI 10.1109/TMC.2021.3125201, IEEE Transactions on Mobile Computing

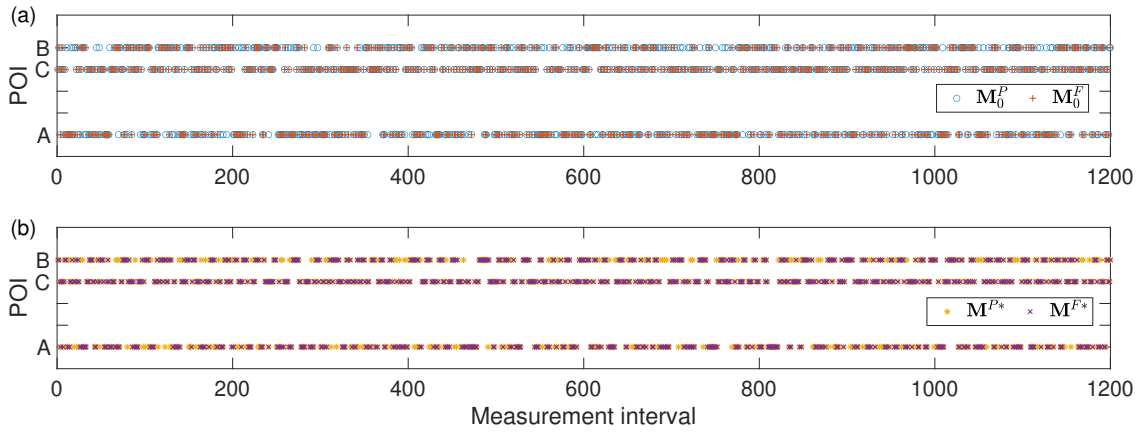

Fig. 5: Comparison of (a) the measurement periods at each POI A, B, C given by one PMD $\mathbb{M}_0^P$ (blue 'o') and the corresponding FMD $\mathbb{M}_0^F$ (red '+'), and (b) those given by the optimal PMD $\mathbb{M}^{P*}$ (yellow '$*$') and the corresponding optimal FMD $\mathbb{M}^{F*}$ (violet '$\times$') after the SA-based optimization process, respectively, where the y-axis is given by the distance with respect to the POI A.

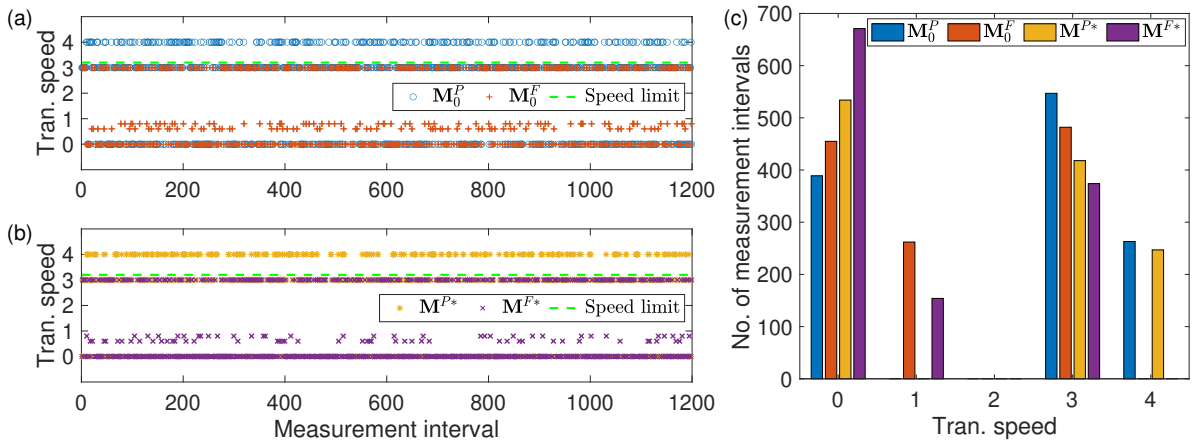

Fig. 6: Comparison of (a) the transition speed of the probe between each measurement interval given by the PMD $\mathbb{M}_0^P$ in Fig. 5 and the corresponding $\mathbb{M}_0^F$, respectively, (b) the same comparison for the optimal PMD $\mathbb{M}^{P*}$ and the corresponding optimal FMD $\mathbb{M}^{F*}$ after the SA-based optimization process, respectively, where the speed limit is marked by the green dashed-line, and (c) the comparison of the number of transition intervals at each required speed regions (i.e., the number 'i' for $i = 0, 1, 2, 3, 4$ denotes the speed region from $i - 0.5$ to $i + 0.5$) for the above four measurement decisions, respectively.

on uniform distribution) from each sub-measurement set $\mathbf{S}_k$ ($k = 1, 2, 3$) to update the PMD $\mathbb{M}_i^P$ and the FMD $\mathbb{M}_i^F$ for the next iteration (See Eqs. (25)–(28) in Subsec. III-A). The cost function of the updated FMD $\mathbb{M}_i^F$ was then calculated and compared to that of the previous FMD $\mathbb{M}_{i-1}^F$, and the FMD $\mathbb{M}_i^F$ was accepted or rejected based on the cost function difference, ΔJ_i, with a probability $P_i = e^{-C\Delta J_i/T_i^{SA}}$, where $C = \frac{1}{\Delta J_i}$ if $i = 1$, and $C = 0.2$ otherwise. The temperature T^{SA} was initially set at $T_1^{SA} = 2.8037$ to keep the probability of accepting a non-decreasing worse solution at the beginning $P_1 = 0.7$, then decrementally reduced via a multiplier $\delta = 0.9970$ until $T_{\min}^{SA} = 0.1390$. This SA-based shuffle-and-pair process was iterated 1,000 times, and the optimal measurement decision $\mathbb{M}^{F*}$ was chosen for the mobile agent to follow in the measurement simulation next.

Finally, the intermittently measured viscoelasticity data at these three POIs, $g_A[\cdot]$, $g_B[\cdot]$, and $g_C[\cdot]$, were obtained by selecting the viscoelasticity values (at these three POIs) in the measurement intervals given by the optimal FMD $\mathbb{M}^{F*}$. The viscoelasticity value at each POI—under the external temperature fluctuation—was recovered using the compressed sensing algorithm via the ℓ_1-minimization in Eq. (30). Also, the so-called *sequential-sensing* method was implemented, where samples were taken sequentially in turn at the three POIs—under the same setup and speed constraint above, and the entire sequence of viscoelasticity data was obtained from the sampled data via linear interpolation. As the sequential-sensing represented the ideal, constraint-free scenario (no constraints other than the mobile speed were imposed, and no requirement of minimizing the cost in the total distance and number of transitions was considered), it served well as a baseline to assess the quality/performance of the proposed

This article has been accepted for publication in a future issue of this journal, but has not been fully edited. Content may change prior to final publication. Citation information: DOI 10.1109/TMC.2021.3125201, IEEE Transactions on Mobile Computing

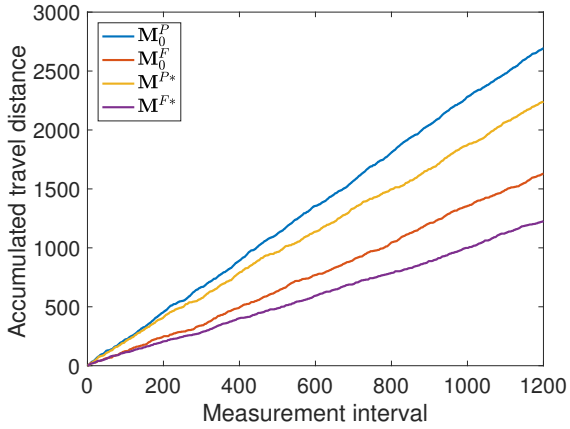

Fig. 7: Comparison of the accumulated agent travel distance in the whole measurement process based on the initial PMD $\mathbb{M}_0^P$, the initial FMD $\mathbb{M}_0^F$, the optimal PMD $\mathbb{M}^{P*}$, and the optimal FMD $\mathbb{M}^{F*}$, respectively.

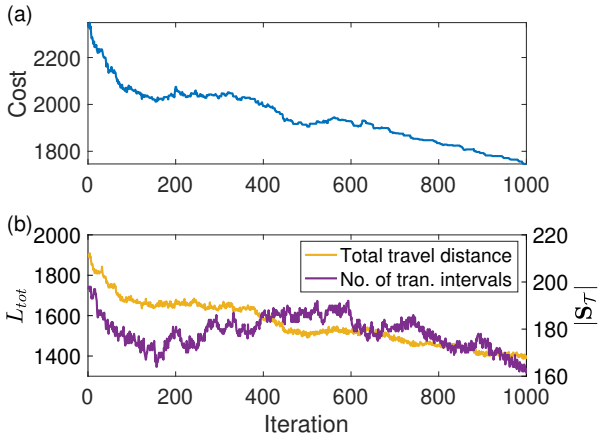

Fig. 8: (a) The cost of each solution, and (b) the total travel distance and the number of the transition-only intervals in the SA process across the 1,000 iterations, respectively.

technique.

To evaluate the effect of the weights c_1 and c_2 in the SA-based optimization process on the sensing performance, the simulation was repeated for $c_1 : c_2 = 100 : 1$ and $c_1 : c_2 = 1 : 100$, respectively. We also examined the performance of the check-and-removal process in maintaining the distribution of the measurement periods between the POIs (Lemma 10 and Theorem 11 in Sec. III). First, for the given distances between the three POIs and the speed of the agent, the neighborhood relation of these three POIs was determined, as shown in Table I and Fig. 4, and then used to determine the probability of taking measurement at each POI in any given p^{th} interval by Lemma 10 (see Eq. (33)), as given blow

$$P_{A,p} = P_{A,1}\left[\left(P_{A,p-1} + P_{C,p-1}\right) + P_{p-1}^{\mathbf{Tr},r}\right], \tag{56}$$

$$P_{B,p} = P_{B,1}\left[\left(P_{B,p-1} + P_{C,p-1}\right) + P_{p-1}^{\mathbf{Tr},r}\right], \tag{57}$$

$$P_{C,p} = P_{C,1}. \tag{58}$$

At POI C, agent R can reach from any POI within one transition interval, thereby, the probability of measuring at POI C in any period was the same as the initial distribution of the measurement interval, $P_{C,1}$. And the probability of having any p^{th} measurement interval for transition was obtained accordingly as

$$P_p^{\mathbf{Tr},r} = 1 - \left(P_{A,p} + P_{B,p} + P_{C,p}\right) \tag{59}$$

The probability of measuring at each POI for each measurement period were computed recursively via Eq. (56) to Eq. (59) for given initial distribution $P_{A,1}$, $P_{B,1}$, $P_{C,1}$. In the simulation, the uniform initial distribution $P_{A,1} = P_{B,1} = P_{C,1} = \frac{1}{3}$ and $P_1^{\mathbf{Tr},r} = 0$ was chosen, and then compared to those obtained for non-uniform initial distributions $P_{A,1} = P_{B,1} = \frac{2}{5}$, $P_{C,1} = \frac{1}{5}$, and $P_{A,1} = \frac{1}{2}$, $P_{B,1} = \frac{1}{3}$, $P_{C,1} = \frac{1}{6}$, respectively.

C. Results and Discussions

The simulation results are presented and discussed below. First, the measurement sequences at each POI given by the initial PMD $\mathbb{M}_0^P$ and the corresponding FMD $\mathbb{M}_0^F$ are compared in Fig. 5(a), respectively, and after the SA-based optimization process, the sequences of the optimal PMD $\mathbb{M}^{P*}$ and the optimal FMD $\mathbb{M}^{F*}$ are also compared in Fig. 5(b), respectively. The required speeds of the agent for each between-POI transition are compared for the PMD $\mathbb{M}_0^P$ and the FMD $\mathbb{M}_0^F$ in Fig. 6(a), where the speed limit of 3 (units per transition interval) is marked (green-dashed line), and zero speed corresponds to no-transition. Correspondingly, the required transition speeds for the optimal PMD and the optimal FMD, $\mathbb{M}^{P*}$ and $\mathbb{M}^{F*}$ respectively, are also compared in Fig. 6(b). The numbers of measurement intervals at each required speed in the above four MDs are compared in Fig. 6(c), where the histogram were all zero at trans. speed=2, because the minimal required speeds, computed by using the distance between the POIs (3 or 4) and the given transition time (I^T or $I^T + I^M = 5I^T$) via Eq. (3), were either in the region of [0,0.5), or [0.5,1.5), or [2.5,3.5), or [3.5,4].

The accumulated transition distance of the mobile agent for PMDs $\mathbb{M}_0^P$ and $\mathbb{M}^{P*}$ and FMDs $\mathbb{M}_0^F$ and $\mathbb{M}^{F*}$ are compared in Fig. 7. The SA-based optimization process was further examined through the progress of the cost function J, the total transition distance L_{tot}, and the total number of intervals for transition $|\mathbf{S}_\mathcal{T}|$ along with the SA iteration process in Fig. 8, respectively. The recovered signals and the errors at the three POIs are compared to the original signals and those obtained via the sequential-sensing method in Fig. 9 (a), (b), respectively. In Fig. 9 (b), the relative 2-norm error was quantified with the DC-component ($E_{\infty,i} = 5$ in Eq. (55)) removed—to better evaluate the three methods for dynamics mapping. The recovery errors of using $c_1 : c_2 = 100 : 1$ and $c_1 : c_2 = 1 : 100$ in the SA-based optimization process are compared in Fig. 10(a), (b), (c) for POI A, B, C, respectively, and the accumulated transition distance of these two cases are compared in Fig. 10(d). Finally, the variation of the probability distribution of the measurement between the POI A, B, C with

This article has been accepted for publication in a future issue of this journal, but has not been fully edited. Content may change prior to final publication. Citation information: DOI 10.1109/TMC.2021.3125201, IEEE Transactions on Mobile Computing

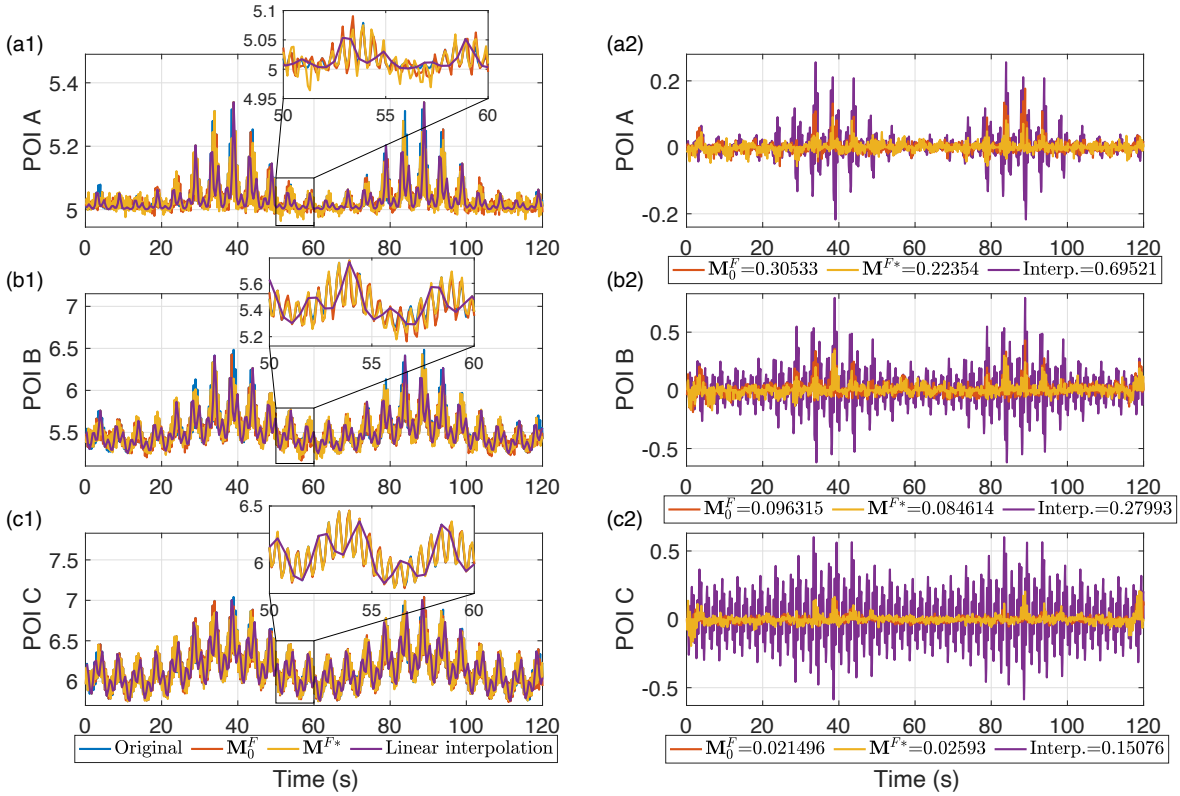

Fig. 9: The recovered results using the initial FMD $\mathbb{M}_0^F$ (red) and the SA optimized FMD $\mathbb{M}^{F*}$ (yellow) are compared to the underlined dynamic signals (blue) and those obtained using the sequential-sensing and linear interpolation (purple) at POIs A (a1), B (b1), and C (c1), respectively (where the inserts show the zoomed-in view). The error of the recovered signals of $\mathbb{M}_0^F$ (red) and $\mathbb{M}^{F*}$ (yellow) with comparison to that obtained via the sequential-sensing at POIs A (a2), B (b2), and C (c2), respectively, with the relative 2-norm errors shown in the legend.

the increase of the interval is compared in Fig. 11, and the expected distribution of the total measurement interval number between the three POIs by Eqs. (56)-(59) are compared to the actual numbers counted in the simulation for the FMD $\mathbb{M}_0^F$ and the optimal FDM $\mathbb{M}^{F*}$ in Fig. 12, respectively. The curves of POI A and POI B in Fig. 11 (a) and (b) overlapped each other, because both the neighborhood relations of these two POIs to POI C and the initial condition were chosen the same.

The simulation results showed that by using the proposed OSMS-DF technique, the temporal-spatial coupling in mobile dynamics sensing was avoided while the sensing performance was optimized (Objectives $\mathcal{O}_1$, $\mathcal{O}_2$, and $\mathcal{O}_4$). First, through the random permutation and partition process, assignment of one interval to multiple POIs was avoided (blue 'o' in Fig. 5(a)). However, as the agent mobility capacity (speed limitation) was not accounted for in the partition, out-of-range transition speed occurred in the PMD $\mathbb{M}_0^P$ obtained—as shown in Fig. 6(a), (c), speed of 4 (over the limit of 3) occurred at over 260 POI-transitions (over 32% of the total transitions). Contrarily, through the proposed check-and-removal process, by using only a small fraction (16.42%) of the intervals for POI-transition, such out-of-range transitions were avoided: As shown in Fig. 5(a), (b), the non-overlapped blue 'o's and red '+'s (representing the transition-only intervals) were only $\sim 16\%$, and no out-of-range transition speed occurred in the FMD $\mathbb{M}_0^F$ obtained (see Fig. 6(a)).

The sensing performance was further enhanced through the proposed SA-based shuffle-and-pair process: First, the number of out-of-range transition speed occurred less in the optimal PMD $\mathbb{M}^{P*}$ than those in the previous PMD $\mathbb{M}_o^P$ (see Fig. 6 (b), (c)). As a result, the accumulated POI-transition distance was reduced by nearly 17% (from 2693 to 2242, see Fig. 7). Consequently, the number of POI-transitions was dramatically reduced (i.e., the number of intervals with zero transition speed dominated, see Fig. 6(c)), so was the accumulated transition distance (reduced from 1630 to 1228, an over 32% reduction, see Fig. 7). Moreover, random "jump" in the SA-optimization process was clearly observed in the simulation, as the cost was not monotonically reduced during the initial phase of the iteration process, but eventually reduced later (Fig. 8(a)). The choice of balanced weights on the transition distance and the number of transition intervals was also clearly observed (Fig. 8(b)). As the number of POIs N^s, in general, was orders of magnitude smaller than the total number of measurements N^t (i.e., in many applications $N^s < 10$ shall be chosen to ensure the recovery quality via the CS method [12]), the N^s increase effect on the convergence of the SA-based optimization tens to be small (as also observed in our simulation when N^s was increased from 3 to 5). Thus, the simulation

This article has been accepted for publication in a future issue of this journal, but has not been fully edited. Content may change prior to final publication. Citation information: DOI 10.1109/TMC.2021.3125201, IEEE Transactions on Mobile Computing

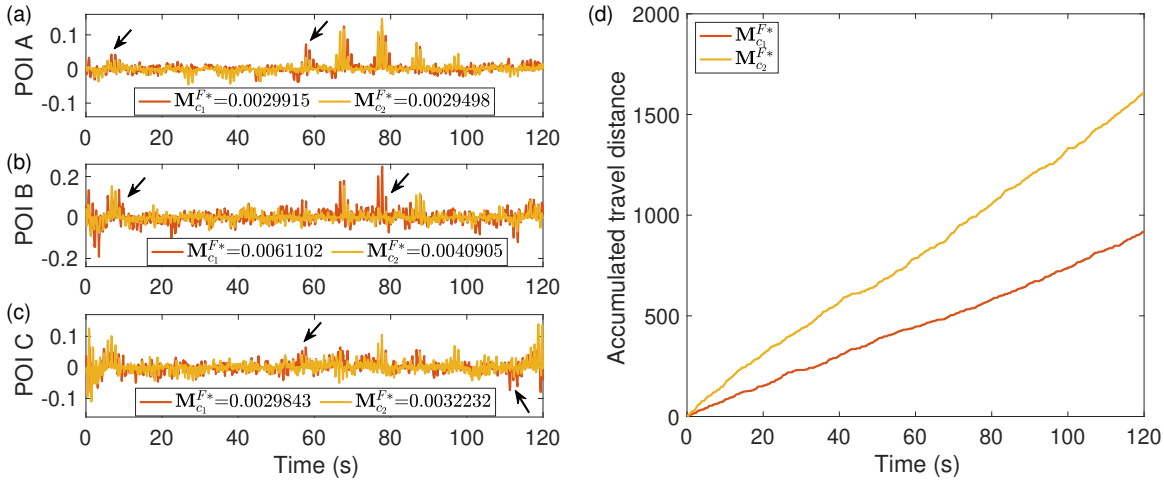

Fig. 10: The error of the recovered signals by the SA optimized FMD $\mathbb{M}_{c_1}^{F*}$ (red) with weight $c_1 : c_2 = 100 : 1$ and by the SA optimized FMD $\mathbb{M}_{c_2}^{F*}$ (yellow) with weight $c_1 : c_2 = 1 : 100$ at POIs A (a), B (b), and C (c), respectively. The relative 2-norm errors are presented in the legend. The arrows point out the where the error of $\mathbb{M}_{c_1}^{F*}$ is clearly larger than that of $\mathbb{M}_{c_2}^{F*}$. (d) The accumulated travel distance of $\mathbb{M}_{c_1}^{F*}$ (red) and $\mathbb{M}_{c_2}^{F*}$ (yellow)

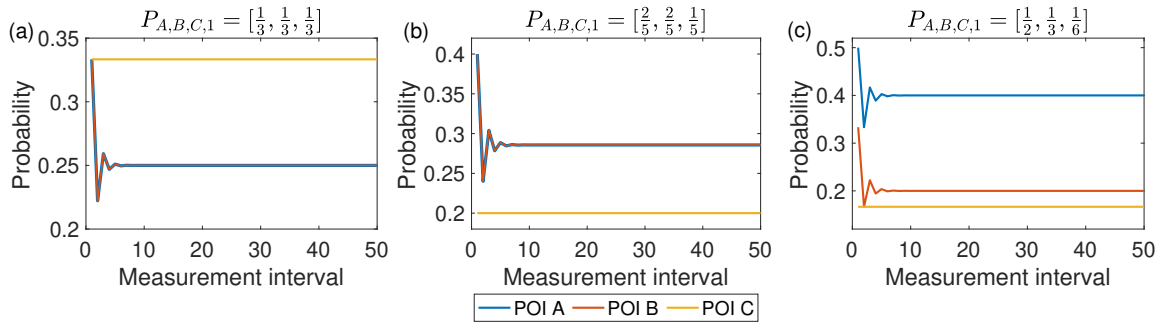

Fig. 11: The first fifty probabilities that the agent R will measure at POIs A, B, and C in the simulation example with different initial distribution probability: (a) uniform initial distribution $P_{A,1} = P_{B,1} = P_{C,1} = \frac{1}{3}$; (b) initial distribution $P_{A,1} = P_{B,1} = \frac{2}{5}$, $P_{C,1} = \frac{1}{5}$; and (c) initial distribution $P_{A,1} = \frac{1}{2}$, $P_{B,1} = \frac{1}{3}$, $P_{C,1} = \frac{1}{6}$, respectively.

results demonstrated the efficacy of the proposed technique in addressing the coupling and optimization requirements in mobile dynamics sensing.

Next, we can see from the simulation that the dynamic viscoelasticity of the sample can be accurately captured by the proposed method. The highest frequency component of the input at 1 Hz implies that the total 1200 measurements over the 120 seconds was enough to capture the dynamic variation at any of the POI—Through the proposed mobile sensing scheme, such a dynamic variation can also be recovered from the intermittently measured data of size ∼300-400 at each POI: The recovered nanomechanical variations at all three POIs by using the FMD $\mathbb{M}_0^F$ followed the "true" dynamics closely, with the relative 2-norm error between 2.5% to 22.4%, respectively (see Fig. 9). On the contrary, when using the sequential-sensing method aliasing in capturing the dynamics at the three POIs was pronounced (see the inserts in Fig. 9 (a)), resulting in much larger errors in capturing the dynamics of the viscoelasticity at the three POIs—the relative 2-norm error was three to six times larger than that when using the proposed technique (see Fig. 9).

Moreover, by using the proposed SA-based optimization, the total transition distance was reduced by over 25% while maintaining the same accuracy (see the results of the optimal FMD $\mathbb{M}^{F*}$ in Fig. 9). The dynamics mapping quality was not effected by the type of distribution used in the random permutation process (Step 2 of the proposed method)—the quality was ultimately determined by the compressed ratio relative to the full length of the sequence attained at each POI. Our simulation results also showed that for ten different types of distribution used in the permutation, same level of mapping quality was achieved. Also, through the SA-based optimization the sensing cost (i.e., the total transition distance) can be traded-off with the sensing quality (i.e., the number of intervals fully used for transition—$|\mathbf{S}_{\mathcal{T}}|$), by tuning the relative size of the weights c_1 vs c_2 in the cost function (Eq. (13)): As shown in Fig. 10, instead of weighting on the measurement error ($c_1 : c_2 = 1 : 100$), an emphasis on the transition distance ($c_1 : c_2 = 100 : 1$) results in much less transition distance (a 42% reduction), at the price of a larger estimation error (as marked out by the errors in Fig. 10(a)-(c)). Therefore, the simulation results demonstrated that mobile sensing of

This article has been accepted for publication in a future issue of this journal, but has not been fully edited. Content may change prior to final publication. Citation information: DOI 10.1109/TMC.2021.3125201, IEEE Transactions on Mobile Computing

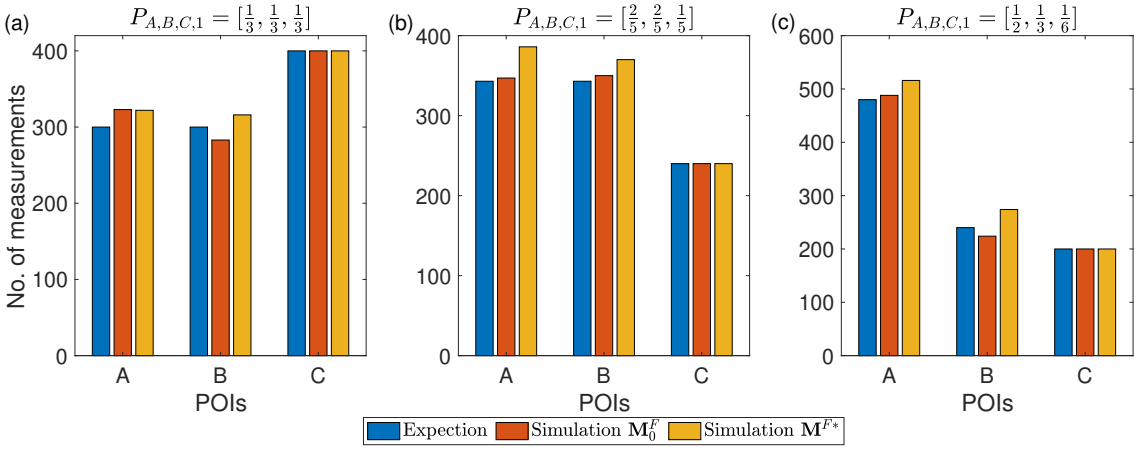

Fig. 12: Number of measurements on POIs A, B, and C with different sets of initial distribution as in the simulation example after check-and-removal process: (a) uniform initial distribution $P_{A,1} = P_{B,1} = P_{C,1} = \frac{1}{3}$; (b) initial distribution $P_{A,1} = P_{B,1} = \frac{2}{5}$, $P_{C,1} = \frac{1}{5}$; and (c) initial distribution $P_{A,1} = \frac{1}{2}$, $P_{B,1} = \frac{1}{3}$, $P_{C,1} = \frac{1}{6}$, respectively.

dynamic processes at multiple POIs can be achieved by using the proposed OSMS-DF technique.

Finally, the simulation validated the theoretical prediction of the measurement interval distribution between the POIs (Lemma 10 and Theorem 11). For the neighborhood relation of the POIs given in Table I, the eigenvalues of the distribution mapping matrix $\widehat{\mathbf{W}}_{\mathcal{H}_0^-}$ in Eq. (46) were computed as $\lambda = [0.3333, -0.3333, 0]$ for the chosen uniform initial distribution. As a result, the measurement distribution vector P_p converged quickly to a constant (see Theorem 11 and Remark 12), as shown in Fig. 11(a). Moreover, it was clear that such a distribution can be tuned through the choice of different initial distribution. For example, by choosing a non-uniform initial distribution of $P_{A,1} = \frac{2}{5}$ and $P_{A,1} = \frac{1}{2}$, the measurement distribution at POI A was changed from 0.25 to 0.29 and 0.4, respectively (See Fig. 11(b) and (c)). The theoretical prediction of the measurement distribution matched those counted in the simulation well—the simulation values for the initial FMD $\mathbb{M}_0^F$ were at most 7% less than the theoretical prediction, and those for the optimal FMD $\mathbb{M}^{F*}$ were all no less than the theoretical prediction, respectively (see Fig. 12). Therefore, the simulation results showed that through the proposed OSMS-DF technique, distribution of the measurement time between the POIs converged, and can be tuned through the choice of initial distribution to ensure and enhance the dynamics recovery at different POIs—for dynamically heterogeneous fields.

VI. Conclusion

In this paper, an optimal mobile sensing algorithm based on compressed sensing is proposed to capture the dynamics variations at multiple POIs by using a mobile agent. A check-and-removal process based on random permutation and partition was developed to remove the spatial-temporal coupling in the dynamics sensing with limited mobile sensing capability. Then a simulated-annealing based shuffle-and-pair process was explored to minimize the total POI-transition distance while preserving the measurement quality. The distribution of the measurement intervals between the POIs was characterized in the probability sense, and converge of the distribution was shown for a simplified case. Simulation study of implementation of the proposed technique in discrete nanomechanical mapping was demonstrated and discussed. For future work, the robustness and performance of the proposed approach can be further improved via online adaptation of the measurement decision, to account for external disturbances and dynamics heterogeneity of the sampling field.

VII. Acknowledgement

The authors would like to gratefully thank the support of NSF grants CMMI-1663055, CMMI-1851907, and IIBR-1952823.

References

[1] Walter HF Smith and David T Sandwell. Global sea floor topography from satellite altimetry and ship depth soundings. *Science*, 277(5334):1956–1962, 1997.

[2] CD Rullan Silva, AE Olthoff, José Antonio Delgado de la Mata, and A Pajares Alonso. Remote monitoring of forest insect defoliation. a review. *Forest Systems*, 22(3):377–391, 2013.

[3] Gabriel A Vecchi, Brian J Soden, Andrew T Wittenberg, Isaac M Held, Ants Leetmaa, and Matthew J Harrison. Weakening of tropical pacific atmospheric circulation due to anthropogenic forcing. *Nature*, 441(7089):73, 2006.

[4] Inbal Becker-Reshef, Chris Justice, Mark Sullivan, Eric Vermote, Compton Tucker, Assaf Anyamba, Jen Small, Ed Pak, Ed Masuoka, Jeff Schmaltz, et al. Monitoring global croplands with coarse resolution earth observations: The global agriculture monitoring (glam) project. *Remote Sensing*, 2(6):1589–1609, 2010.

[5] Andrew K Jorgenson and Kennon A Kuykendall. Globalization, foreign investment dependence and agriculture production: Pesticide and fertilizer use in less-developed countries, 1990–2000. *Social Forces*, 87(1):529–560, 2008.

[6] Jorge Cortes, Sonia Martinez, Timur Karatas, and Francesco Bullo. Coverage control for mobile sensing networks. *IEEE Transactions on robotics and Automation*, 20(2):243–255, 2004.

[7] María Santos, Yancy Diaz-Mercado, and Magnus Egerstedt. Coverage control for multirobot teams with heterogeneous sensing capabilities. *IEEE Robotics and Automation Letters*, 3(2):919–925, 2018.

[8] Brent Schlotfeldt, Dinesh Thakur, Nikolay Atanasov, Vijay Kumar, and George J Pappas. Anytime planning for decentralized multirobot active information gathering. *IEEE Robotics and Automation Letters*, 3(2):1025–1032, 2018.

[9] Micah Corah and Nathan Michael. Distributed matroid-constrained submodular maximization for multi-robot exploration: Theory and practice. *Autonomous Robots*, 43(2):485–501, 2019.

[10] Zhenyu Zhou, Junhao Feng, Bo Gu, Bo Ai, Shahid Mumtaz, Jonathan Rodriguez, and Mohsen Guizani. When mobile crowd sensing meets uav: Energy-efficient task assignment and route planning. *IEEE Transactions on Communications*, 66(11):5526–5538, 2018.

[11] David L Donoho. Compressed sensing. *IEEE Transactions on information theory*, 52(4):1289–1306, 2006.

[12] Emmanuel J Candès and Michael B Wakin. An introduction to compressive sampling. *IEEE signal processing magazine*, 25(2):21–30, 2008.

[13] Emmanuel J Candes, Justin K Romberg, and Terence Tao. Stable signal recovery from incomplete and inaccurate measurements. *Communications on Pure and Applied Mathematics: A Journal Issued by the Courant Institute of Mathematical Sciences*, 59(8):1207–1223, 2006.

[14] Xuemei Li, Yuyan Deng, and Lixing Ding. Study on precision agriculture monitoring framework based on wsn. In *2008 2nd International Conference on Anti-counterfeiting, Security and Identification*, pages 182–185. IEEE, 2008.

[15] Minh T Nguyen, Hung M La, and Keith A Teague. Collaborative and compressed mobile sensing for data collection in distributed robotic networks. *IEEE Transactions on Control of Network Systems*, 5(4):1729–1740, 2017.

[16] Haifeng Zheng, Jiayin Li, Xinxin Feng, Wenzhong Guo, Zhonghui Chen, and Neal Xiong. Spatial-temporal data collection with compressive sensing in mobile sensor networks. *Sensors*, 17(11):2575, 2017.

[17] Xiangping Gu, Xiaofeng Zhou, Baohua Yuan, and Yanjing Sun. A bayesian compressive data gathering scheme in wireless sensor networks with one mobile sink. *IEEE Access*, 6:47897–47910, 2018.

[18] Shriram Sarvotham, Dror Baron, Michael Wakin, Marco F Duarte, and Richard G Baraniuk. Distributed compressed sensing of jointly sparse signals. In *Asilomar conference on signals, systems, and computers*, pages 1537–1541, 2005.

[19] Swatantra Kafle, Vipul Gupta, Bhavya Kailkhura, Thakshila Wimalajeewa, and Pramod K Varshney. Joint sparsity pattern recovery with 1-b compressive sensing in distributed sensor networks. *IEEE Transactions on Signal and Information Processing over Networks*, 5(1):15–30, 2018.

[20] Liwen Xu, Xiaohong Hao, Nicholas D Lane, Xin Liu, and Thomas Moscibroda. Cost-aware compressive sensing for networked sensing systems. In *Proceedings of the 14th international conference on Information Processing in Sensor Networks*, pages 130–141, 2015.

[21] Emmanuel J Candes. The restricted isometry property and its implications for compressed sensing. *Comptes rendus mathematique*, 346(9-10):589–592, 2008.

[22] Scott Kirkpatrick, C Daniel Gelatt, and Mario P Vecchi. Optimization by simulated annealing. *science*, 220(4598):671–680, 1983.

[23] Tianwei Li, Qingze Zou, Tianxing Ma, Jonathan Singer, and Chanmin Su. Adaptive simultaneous topography and broadband nanomechanical mapping of heterogeneous materials on atomic force microscope. *IEEE Transactions on Nanotechnology*, 19:689–698, 2020.

[24] Jingren Wang, Xuemei Li, Qingze Zou, Chanmin Su, and Nicole S Lin. Rapid broadband discrete nanomechanical mapping of soft samples on atomic force microscope. *Nanotechnology*, 31(33):335705, 2020.

[25] Pauline Durand-Smet, Nicolas Chastrette, Axel Guiroy, Alain Richert, Annick Berne-Dedieu, Judit Szecsi, Arezki Boudaoud, Jean-Marie Frachisse, Mohammed Bendahmane, Oliver Hamant, et al. A comparative mechanical analysis of plant and animal cells reveals convergence across kingdoms. *Biophysical journal*, 107(10):2237–2244, 2014.

[26] HP Lang, M Hegner, E Meyer, and Ch Gerber. Nanomechanics from atomic resolution to molecular recognition based on atomic force microscopy technology. *Nanotechnology*, 13(5):R29, 2002.

[27] David L Donoho and Xiaoming Huo. Uncertainty principles and ideal atomic decomposition. *IEEE transactions on information theory*, 47(7):2845–2862, 2001.

[28] Emmanuel Candes and Justin Romberg. Sparsity and incoherence in compressive sampling. *Inverse problems*, 23(3):969, 2007.

[29] Jarvis Haupt, Waheed U Bajwa, Michael Rabbat, and Robert Nowak. Compressed sensing for networked data. *IEEE Signal Processing Magazine*, 25(2):92–101, 2008.

[30] Ponnambalam Kumaraswamy. A generalized probability density function for double-bounded random processes. *Journal of Hydrology*, 46(1-2):79–88, 1980.

[31] David L Applegate, Robert E Bixby, Vasek Chvatal, and William J Cook. *The traveling salesman problem: a computational study*. Princeton university press, 2006.

[32] Emmanuel Candes and Justin Romberg. l1-magic: Recovery of sparse signals via convex programming. *URL: www. acm. caltech. edu/l1magic/downloads/l1magic. pdf*, 4:14, 2005.

[33] Josef Stoer and Roland Bulirsch. *Introduction to numerical analysis*, volume 12. Springer Science & Business Media, 2013.

[34] Sean P Meyn and Richard L Tweedie. *Markov chains and stochastic stability*. Springer Science & Business Media, 2012.

[35] Zhonghua Xu, Derek Tramp, Qingze Zou, Pranav Shrotriya, and Ping Xie. Nanoscale broadband viscoelastic spectroscopy of soft materials using iterative control. *Experimental mechanics*, 52(7):757–769, 2012.

[36] Hal F Brinson, L Catherine Brinson, et al. Polymer engineering science and viscoelasticity. *An introduction*, 2008.